THE MICROWAVE RADIOMETER AS A REMOTE SENSING INSTRUMENT

W.H. Peake

The Ohio State University

ElectroScience Laboratory

(formerly Antenna Laboratory)
Department of Electrical Engineering
Columbus, Ohio 43212

TECHNICAL REPORT 1903-8
17 January 1969

Contract Number NSR-36-008-027

National Aeronautics and Space Administration
Office of Grants and Research Contracts
Washington, D.C. 20546

NOTICES

When Government drawings, specifications, or other data are used for any purpose other than in connection with a definitely related Government procurement operation, the United States Government thereby incurs no responsibility nor any obligation whatsoever, and the fact that the Government may have formulated, furnished, or in any way supplied the said drawings, specifications, or other data, is not to be regarded by implication or otherwise as in any manner licensing the holder or any other person or corporation, or conveying any rights or permission to manufacture, use, or sell any patented invention that may in any way be related thereto.

The Government has the right to reproduce, use, and distribute this report for governmental purposes in accordance with the contract under which the report was produced. To protect the proprietary interests of the contractor and to avoid jeopardy of its obligations to the Government, the report may not be released for non-governmental use such as might constitute general publication without the express prior consent of The Ohio State University Research Foundation.

REPORT 1903-8

REPORT
by
THE OHIO STATE UNIVERSITY ELECTROSCIENCE LABORATORY
(Formerly Antenna Laboratory)
COLUMBUS, OHIO 43212

Sponsor	National Aeronautics and Space Administration Office of Grants and Research Contracts Washington, D.C. 20546
Contract Number	NSR-36-008-027
Investigation of	Radar and Microwave Radiometric Techniques for Geoscience Experiments
Subject of Report	The Microwave Radiometer as a Remote Sensing Instrument
Submitted by	W.H. Peake ElectroScience Laboratory Department of Electrical Engineering
Date	17 January 1969

ABSTRACT

This report reviews the fundamentals of microwave radiometry, including radiation theory, antenna effects and instrument design. The parameters of a surface which control its brightness temperature at microwave frequencies are reviewed and related to other parameters which characterize the surface. Among these, the role of the complex dielectric constant and its dependence on moisture and ion content, and the effects of surface roughness are discussed. A number of observations of the brightnesss temperature of terrestrial surfaces are reviewed, interpreted on the basis of model surface properties, and considered as potential applications of the instrument as a remote sensor.

CONTENTS

THE MICROWAVE RADIOMETER AS A REMOTE SENSING INSTRUMENT

I. INTRODUCTION

Although imaging microwave radiometers were first developed almost a decade ago, it is only in the last year or so that imagery of reasonable quality has been accessible to the general scientific public. Thus it is still premature to speak of the applications of microwave radiometry to remote sensing. The empirical studies of correlation between features of the imagery and those of the terrain it represents, the development of detailed correspondences between observed radiometric temperatures and significant physical properties of the surface, the quantitative interpretation of those temperatures in terms of the electrical and structural properties of the surface, in short, all of the supporting studies which can convert an interesting picture into a scientific tool are as yet in their infancy.

Nor is it likely, given the particular limitations of this sensor, that it can ever occupy the role of photographic, radar, or infrared imagery. Nevertheless, there are a number of questions, particularly those involving the distribution of water in the upper few meters of the earth's surface, to which the microwave radiometer may make significant contributions. It must certainly be expected that, as with other sensors, experience with the imagery will lead to many applications not now obvious.

This survey, it is hoped, will provide the kind of background information that will allow the geoscientist to make more effective use of the forthcoming imagery. The first sections review the nature of thermal radiation at microwave frequencies, and the characteristics of the instrument used to measure it. We have then tried to show how the attenuation in and thermal emission from the atmosphere degrades the imagery, and how the surface roughness and dielectric constant (particularly the dielectric constant of water) determine the radiometer output. A final rather brief section is concerned with the applications of the imagery.

II. THERMAL RADIATION AT MICROWAVE FREQUENCIES; ANTENNA PARAMETERS

It is well known that every body at a finite temperature emits electromagnetic radiation over a wide range of frequencies and polarizations, and that both the total radiated power and the power in any spectral band increases with the temperature of the body. The nature of this radiation is best described by considering a volume (hohlraum) enclosed by walls maintained at some temperature T (see Fig. 1). If we now consider a small area dA within this isothermal enclosure, a certain amount of energy will flow through dA in a short time dt. If

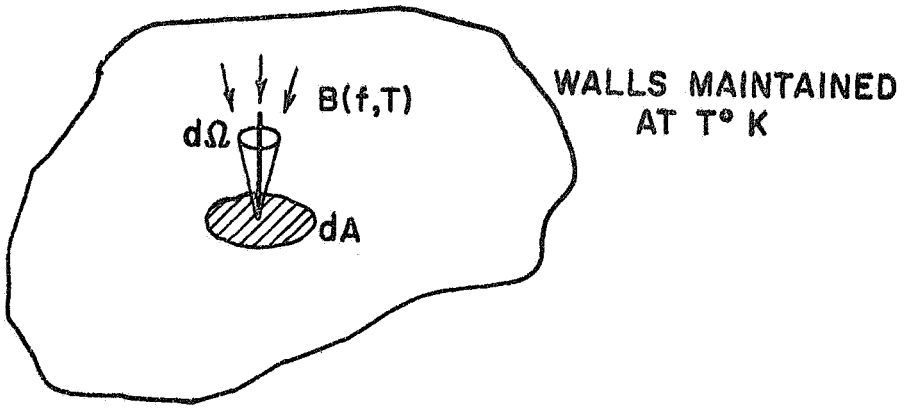

Fig. 1. Radiation in an isothermal enclosure.

we ask how much of this energy has frequencies in the small interval df between f and f + df, and is coming towards dA from within a small cone of solid angle dΩ about the normal to dA, then we find

(1) $$dE = B(f,t)\, dA df dt d\Omega$$

where the constant of proportionality B(f,t) (watts-meter^{-2} - steradian^{-1} - Hertz^{-1}) is referred to as the "specific intensity" or "spectral brightness" of the thermal radiation for that temperature and frequency. It is a consequence of Planck's radiation law that for the black-body radiation within the enclosure, B(f,t) has the form

(2) $$B(f,T) = (2hf^3/c^2)\, [\, \exp(hf/kT) - 1]^{-1}$$

where h is Planck's constant, c is the velocity of light in vacuum, k is Boltzmann's constant, and f is the frequency in Hertz (or cycles/sec as it used to be called). At microwave frequencies, (say f = 1 GHz or 10^9 cps to f = 100 GHz or 10^{11} cps) the quantity hf/kT is usually much less than 1, and (2) can be replaced by the Rayleigh-Jeans formula

(3) $$B(f,T) = 2kT/\lambda^2$$

where $\lambda = c/f$ is the wavelength of the radiation. This approximation to (2) is good to better than 3% if the frequency in GHz is less than T in ^{o}K. Now at microwave frequencies the radiometer measures power, i.e., a quantity proportional to B(f,T), but because of the simple relation between power and temperature implied by (3), it is customary

to adopt the convention that (3) is always correct and to express the measured power as a "brightness temperature" T_b through the relation

$$(4) \qquad T_b = \frac{\lambda^2}{2K}\left(\frac{dE}{dA\ df\ dt\ d\Omega}\right)$$

where dA, df, dt, dΩ become instrumental parameters (collecting aperture, frequency bandwidth, integration time, beam solid angle, respectively). In fact even this step is often avoided by calibrating the radiometer directly in terms of brightness temperature, e.g., by using an emitting body, often a resistor, at a known temperature as a reference.

To see better how this collected power can be treated directly as a temperature, and to introduce some of the parameters which describe the antenna used to collect it, consider next a typical receiving antenna immersed in thermal radiation. It is a fundamental property of an antenna that if an electromagnetic wave of appropriate polarization and intensity S watts/meter^2 is incident on it from direction θ, then the antenna delivers SA(θ) watts to a matched load, (that is, to the radiometer receiver), where A(θ) is referred to as the collecting aperture (meter^2) of the antenna. Intuitively one would expect A(θ) to be equal to the projected area of the antenna, and this is roughly true for many large antennas. Now if A_m is the maximum value of A(θ) then we can write

$$(5) \qquad A(\theta) = A_m f(\theta) \qquad f < 1$$

where f(θ) is the antenna power pattern. But since, for blackbody radiation, the power per unit area coming towards the antenna from within a small cone dΩ in direction θ, and in the frequency interval df is $S = B(f,T)df\ d\Omega$, then the power collected by the antenna from all directions is (see Fig. 2)

$$(6) \qquad dP_a = \frac{1}{2}\int S(\theta)\ A(\theta) d\Omega = \frac{A_m k\ df}{\lambda^2}\int T_b(\theta)\ f(\theta)\ d\Omega$$

where the factor of 1/2 is inserted because the antenna accepts only radiation of one particular polarization whereas the thermal radiation is randomly polarized. Now consider the transmission line connecting the antenna to the matched resistor representing the input to the receiver. This resistor is also a source of random noise and if it is maintained at some temperature T_r, it will deliver $dP_r = KT_r df$ watts to the transmission line (the so-called Johnson noise) in the frequency interval between f and f + df. (The transmission line is the one-dimensional analogue of the hohlraum of the first figure.) Thus associated with a power flow dP_r in a transmission line, there is a "temperature" T_r defined by $T_r \equiv dP_r/kdf$. Consequently we say that

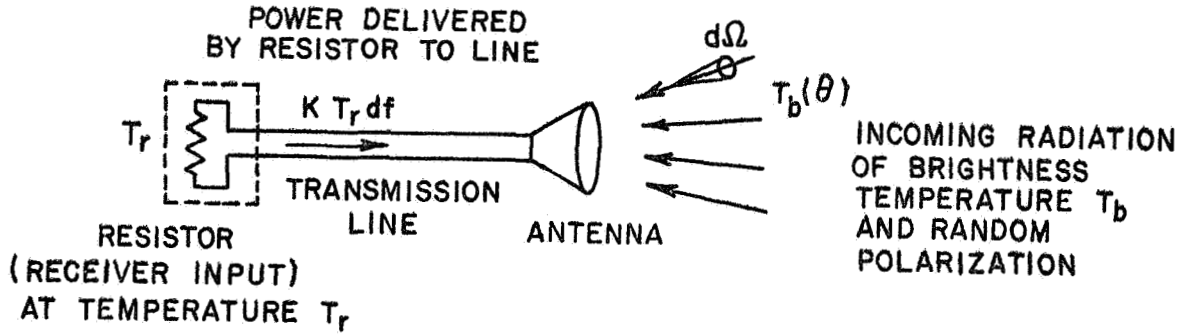

Fig. 2. Radiation absorbed by an antenna.

the power dP_a collected by the antenna represents radiation of temperature T_a,

$$(7) \qquad T_a \equiv \frac{dP_a}{kdf} = \frac{A_m}{\lambda^2} \int f(\theta)\, T_b(\theta)\, d\Omega \quad .$$

The quantity T_a is referred to as the "antenna temperature"; it has nothing to do with whether the antenna is hot or cold, but merely represents the power collected by the antenna as an equivalent radiation temperature via the definition (7).

Now in thermodynamic equilibrium, $T_r = T_b = T$, (i.e., when the receiver load is at the same temperature as the isothermal enclosure, and $T_b(\theta)$ is independent of θ) the same amount of power must flow from antenna to load as from load to antenna. Thus

$$(8) \qquad T = \frac{A_m}{\lambda^2} T \int f(\theta)\, d\Omega \quad \text{or} \quad A_m = \lambda^2 / \int f(\theta)\, d\Omega$$

so that, in general, when the brightness temperature incident on the antenna $T_b(\theta)$ does depend on direction, the antenna temperature becomes

$$(9) \qquad T_a = \frac{\int f(\theta)\, T_b(\theta)\, d\Omega}{\int f(\theta)\, d\Omega} \quad .$$

This quantity is what a microwave radiometer measures; it is the weighted average of the brightness temperature incident on the antenna, the weighting function being the antenna power pattern $f(\theta)$. For a

well designed narrow beam antenna pattern, T_a is nearly equal to the brightness temperature in the direction of the beam, and under reasonably stable environmental conditions can be estimated fairly accurately. In general, however, particularly if the value of T_b is required to high absolute accuracy, the integral equation (9) must be inverted. Procedures are described by Bracewell and Twomey.

A. Antenna Parameters

There are a number of simple relations between the power pattern $f(\theta)$ and the intuitive properties of an antenna such as its beam width. We review these briefly in order to introduce the standard nomenclature. Consider first a typical high gain antenna pattern $f(\theta,\phi)$. The pattern depends on two polar angles (see Fig. 3c), as does the brightness temperature in (9); it is customary to present (see Fig. 3a) only a cross section of the actual pattern function. The beam width of the antenna is usually taken to be the angular separation between the two half power points, (f=1/2). It may be different in the two planes, i.e., the beam may have an elliptical cross section. It is approximately true that, for the large aperture antennas encountered in radiometry, $\theta_B \doteq (d/\lambda)^{-1}$ rad. where d is the diameter of the antenna; and the solid angle Ω_B subtended by the beam is $\Omega_B \doteq \lambda^2/A$ where A is the physical area of the antenna. The maximum collecting aperture A_m is roughly 70% to 80% of the physical area. The final parameter of interest is the directivity D, where

$$(10) \qquad D = \frac{\text{maximum power density radiated by antenna}}{\text{average power density radiated by antenna}}$$

$$D = \frac{f_{max}(\theta,\phi)}{\frac{1}{4\pi}\int f(\theta,\phi)\,d\Omega} = \frac{4\pi}{\int f(\theta,\phi)\,d\Omega} = \frac{4\pi A_m}{\lambda^2}$$

since $f_{max} = 1$. Again, intuitively, $\Omega_B = 4\pi/D$ and this is sometimes used as a definition of the solid angle Ω_B subtended by the main beam. Because of (8) we also have that $A_m = D\lambda^2/4\pi$. We have here ignored the difference between directivity and gain G, defined as $G = \eta D$ (where η is the efficiency of the antenna) since efficiency is extremely high ($\eta > 0.98$) for large antennas.

B. Ray Temperatures; Attenuation in the Medium; Optical Depth

So far we have considered only the brightness temperature of the radiation actually reaching the antenna. In practice, the source of radiation is far removed and the rays must pass through some intervening medium (the atmosphere) which will absorb part of the ray, and which may also emit radiation of its own. Consider (see Fig. 4) a source of thermal radiation, emitting power at a brightness temperature T which then passes through an attenuating layer of thickness dz, a distance z from the source, with power attenuation coefficient a(z) (meter^{-1}). The power per unit area arriving at the layer is $P(z) = B(f,T(z))df\, d\Omega$ and the power lost by absorption or scattering is (definition of a(z)) $dP = -a(z)dz\, P(z)$. This equation is easily integrated to yield

$$(11) \qquad P(z) = P_\infty e^{-\int_0^z a(x)dx} = P_\infty e^{-\tau(z)}$$

where $\tau(z) \equiv \int_0^z a(x)dx$ is the "optical depth" of the attenuating layer between z and the source. Thus the temperature $T_b(\ell)$ of the radiation reaching the receiver at ℓ is $T_b(\ell) = T_\infty e^{-\tau(\ell)}$. If the layer at z also is warm, with physical temperature T(z) (as measured by a thermometer) it will emit thermal radiation in proportion to its emissivity or emission coefficient e(z). The amount of power dP_e emitted is $dP_e = B(T,F)e(z)df\, d\Omega\, dz$ (definition of e(z)). Not all of this reaches the receiver, since it is attenuated by the factor

$$e^{-\int_z^\ell a(x)dx}.$$

Thus the temperature of the radiation reaching ℓ from emission all along the path is

$$(12) \qquad T_e(\ell) = \int_0^\ell T(z)\, e(z)\, e^{-\int_z^\ell a(x)\, dx}\, dz$$

and the total brightness temperature of the radiation reaching the receiver at ℓ is

$$(13) \qquad T_b(\ell) = T_\infty e^{-\tau(\ell)} + \int_0^\ell T(z)\, e(z)\, e^{-\int_z^\ell a(z)dz}\, dz$$

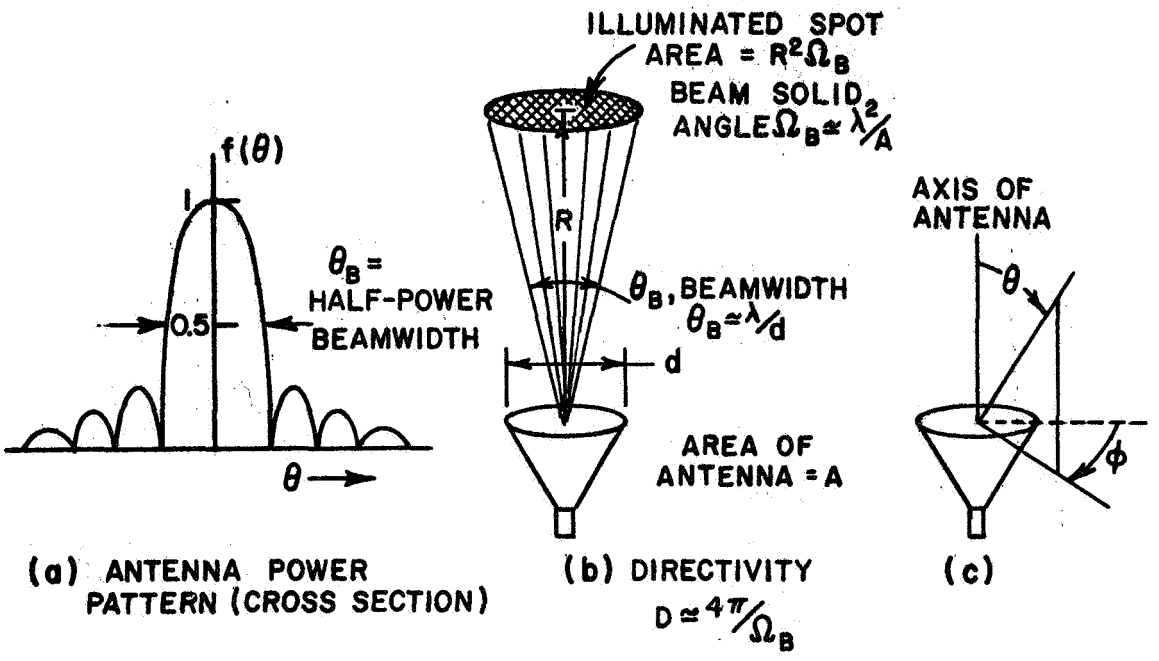

Fig. 3. Antenna parameters.

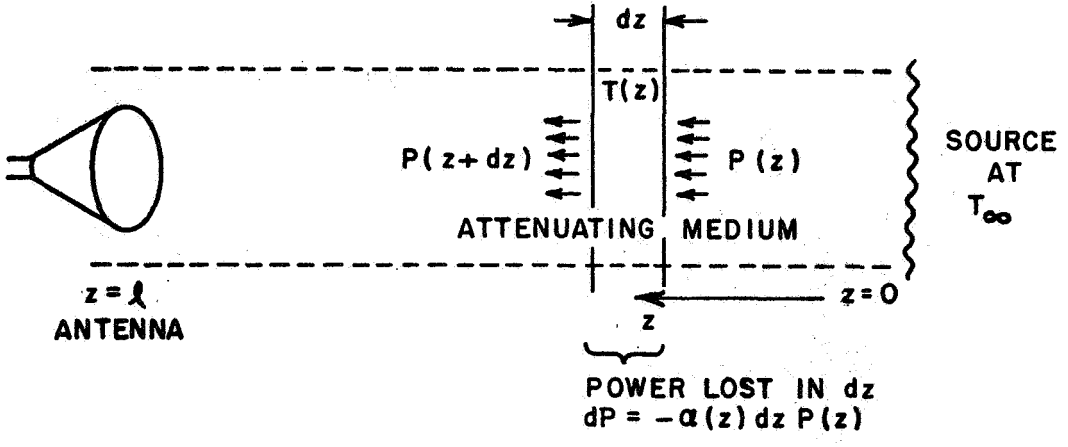

Fig. 4. Effects of attenuation and emission in the path.

In the case where e(z), a(z) and T(z) = T are constants, this reduces to

$$(14) \qquad T_b(\ell) = T_\infty e^{-\tau(\ell)} + T \frac{e}{a} (1 - e^{-\tau(\ell)}).$$

In the case where scattering by the intervening medium is insignificant, e = a and we have

$$(15) \qquad T_b(\ell) = T_\infty e^{-\tau(\ell)} + T(1 - e^{-\tau(\ell)}).$$

This form is often used to express the effect of the transmission line between antenna and receiver, and of the atmosphere between source and receiver, but its restrictions (uniform temperature, uniform attenuation, no scattering) should not be forgotten. It may also be mentioned that (13), with e(z) = a(z) is often used to determine the temperature of radiation emerging from a flat surface when the temperature distribution beneath the surface is not uniform; the expression (13) must be multiplied by the power transmission coefficient through the boundary in this case.

III. THE INSTRUMENT

A microwave radiometer is designed to measure the thermal noise power delivered to it by the antenna. There are two basic configurations (see Fig. 5) commonly used, the unmodulated or straight video receiver, and the modulated or "Dicke" type receiver. In each type, the r.f. amplifier and/or the mixer-i.f. amplifier may be absent. The essential difference between the two types is that the first is simply a power meter whereas in the Dicke type the receiver is alternately switched to look first at the antenna and then at a load maintained at a stable reference temperature. The resulting signal is later detected in a synchronous detector (phase-coherent detector, phase-sensitive demodulator) driven in synchronism with the switch. Although the basic sensitivities of the two systems are comparable, the Dicke type is much less affected by gain fluctuations in the electronics, and is essential where relatively long integration times are required. The video type is often preferred for measuring short bursts of high intensity radiation, as from hot plasmas.

The sensitivity of the radiometer may most easily be estimated by considering the radio frequency input to be a random noise signal of band width df cycles/second. Such a signal permits 2df independent estimates of its amplitude per second. Now if the output of the video detector is averaged for a period of τ seconds (integrator time constant) the number of independent estimates of the power in each measurement period will be $N = 2\tau df$. The precision in measuring the input power is $1/\sqrt{N}$ and this in turn is equal to the precision in measuring the input temperature T_{in}. Thus $\Delta T/T_{in} = \text{const}/\sqrt{\tau\, df}$, or

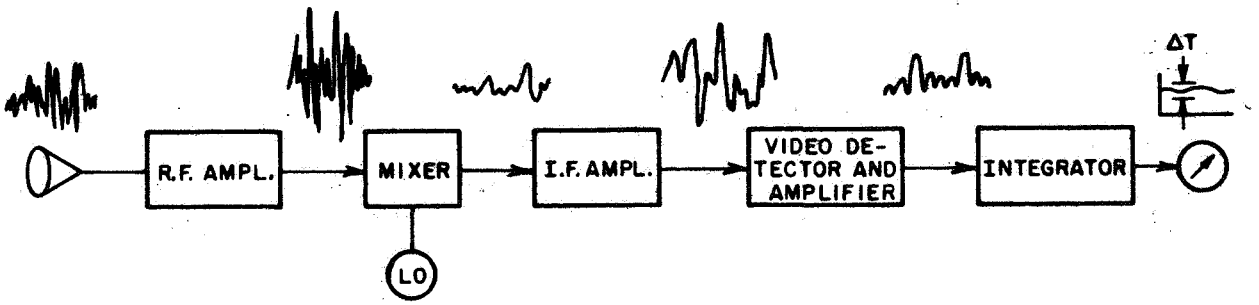

(a) UNMODULATED (VIDEO) RADIOMETER

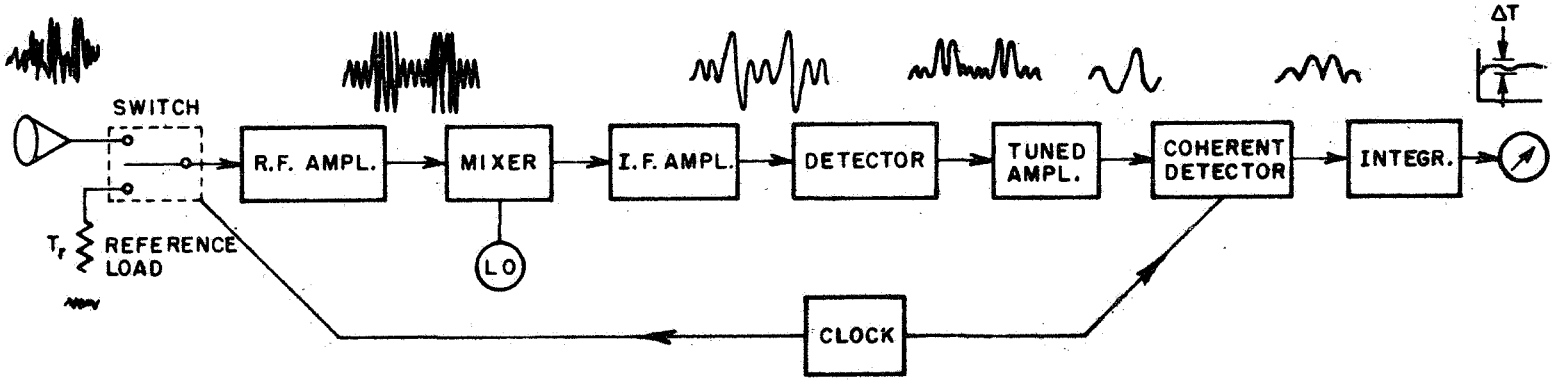

(b) MODULATED (DICKE) RADIOMETER

Fig. 5. Radiometer configuration.

$$(17) \qquad \Delta T = \frac{K_1 T_{in}}{\sqrt{\tau \, df}}$$

where K_1 is a constant depending on the nature of the system. For a straight video receiver, $K_1 = 1$; for a Dicke receiver with square wave modulation and narrow band amplifier, $K_1 = 2.2$. The input temperature T_{in} in not the antenna temperature, but the total input noise temperature taking into account the noise generated within the receiver (usually in the first stage). It is customary to write T_{in} in the form

$$(18) \qquad T_{in} = 290 \ (F-1) + T_a \quad {}^{o}K$$

where T_a is the antenna temperature (usually between $10^{o}K$ and $300^{o}K$ for radiometers viewing the earth) and F is the "noise figure" of the receiver (i.e., 290 (F-1) is the temperature of the noise power attributable to the receiver.) Modern receivers, particularly those with cooled input stages, may have F = 1.3 to 2 at the lower microwave frequencies; conventional mixers, particularly at the higher frequencies, may have F considerably greater than 20. As an example of (17) suppose a receiver has a noise figure F = 4, and an antenna temperature $T_a = 290^{o}K$, so that $T_{in} = 1160^{o}K$. If the predetection band width is df = 400 MHz and the postdetection time constant is $\tau = 0.01$ seconds, then $\Delta T \simeq 1.3^{o}K$. Thus antenna temperatures can be measured to a precision of about $2^{o}K$. This is somewhat better than typical modern imaging radiometers.

We can now discuss briefly the trade-off of design parameters in the radiometer system of most interest to geoscientists, the airborne or satellite borne scanning imager (see Fig. 6). The prototype of this system carries an antenna which rotates its beam about some axis making an angle θ_0 with respect to the vertical. The beam then scans along the ground almost perpendicular to the line of flight at a certain rate; the output of the radiometer is used to modulate the intensity of the beam of a cathode ray tube, or a spot of light on a film. The horizontal motion of the spot is correlated with the swinging antenna beam. The vertical motion of the spot could be correlated with the forward motion of the aircraft. It is customary, however, to use a spot which scans in one direction only and to move the film past the line scan at a rate determined by the height/forward velocity ratio of the aircraft. Thus a continuous strip of image is generated.

The dilemma of system design is now apparent. For good ground resolution, a narrow beam is required. This in turn requires a high scan rate for comparable resolution across and along the flight path. Thus the integration time must be short, and ΔT large. It is not hard to show that for a total scan angle of about one radian, and a depression angle of 45^{o}, the product of beam width θ_B and temperature sensivitity ΔT is given by

(19) $$\theta_B \Delta T \simeq 2K_1 T_{in} \sqrt{\frac{V/H}{(df)}}$$

where V is the vehicle velocity and H the altitude. Since for a given class of vehicle (particularly satellites) the ratio V/H does not vary much, and T_{in} can never be smaller than the antenna temperature, the product $\theta_B \Delta T$ is rather inflexible. Contemporary imagers operate with the product $\Delta T \theta_B$ in the range 4 to 15 (^oK - degrees).

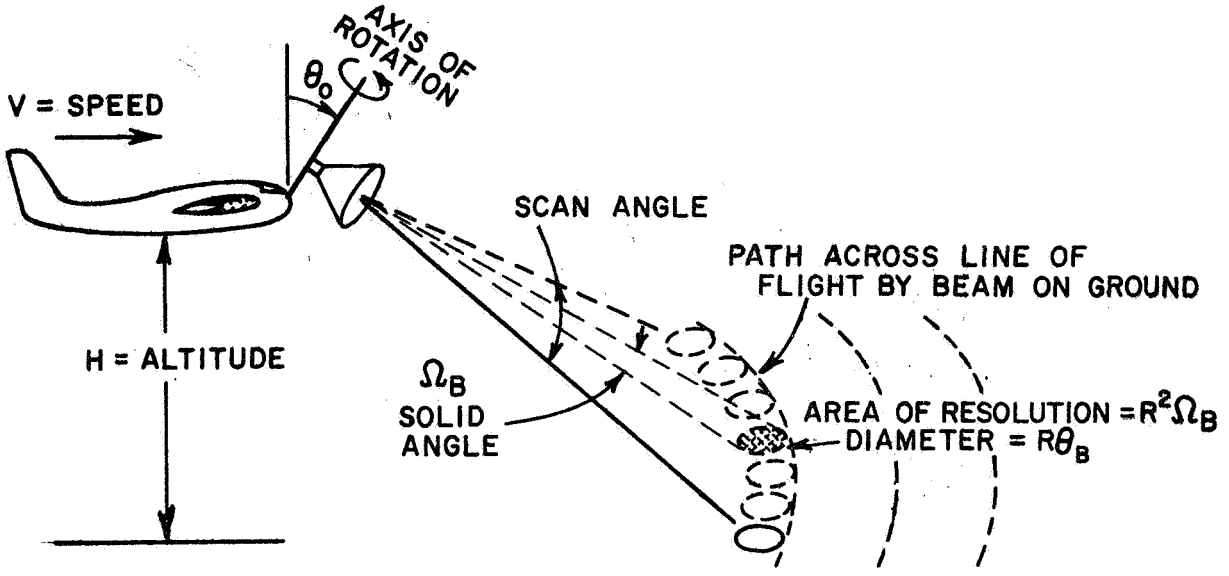

Fig. 6. Imaging system.

IV. THE ATMOSPHERE

We have previously mentioned the influence of an absorbing medium between the source of thermal radiation and the antenna. All terrestrial radiometers must contend with the earth's atmosphere, which has very complex emission and absorption characteristics at microwave frequencies. It is sufficient here to review the behavior of the two principal contributors to atmospheric absorption namely O_2 with a broad line at about 60 GHz, and water vapor, which has a somewhat weaker line at 22.2 GHz. (The O_2 line is actually a multiplet, the individual components being observable only at high altitudes.) Figure 7 shows the sea level absorption coefficient of O_2 alone, for water vapor alone, and for an atmosphere of moderate humidity. Figure 8 shows the corresponding ray temperatures for several standard atmospheric conditions. The one way attenuation, $e^{-\tau_o}$ or optical depth τ_o of the atmosphere may be estimated roughly by putting $T_{ant} = T_{eff}(1-e^{-\tau_o})$ where T_{ant} is

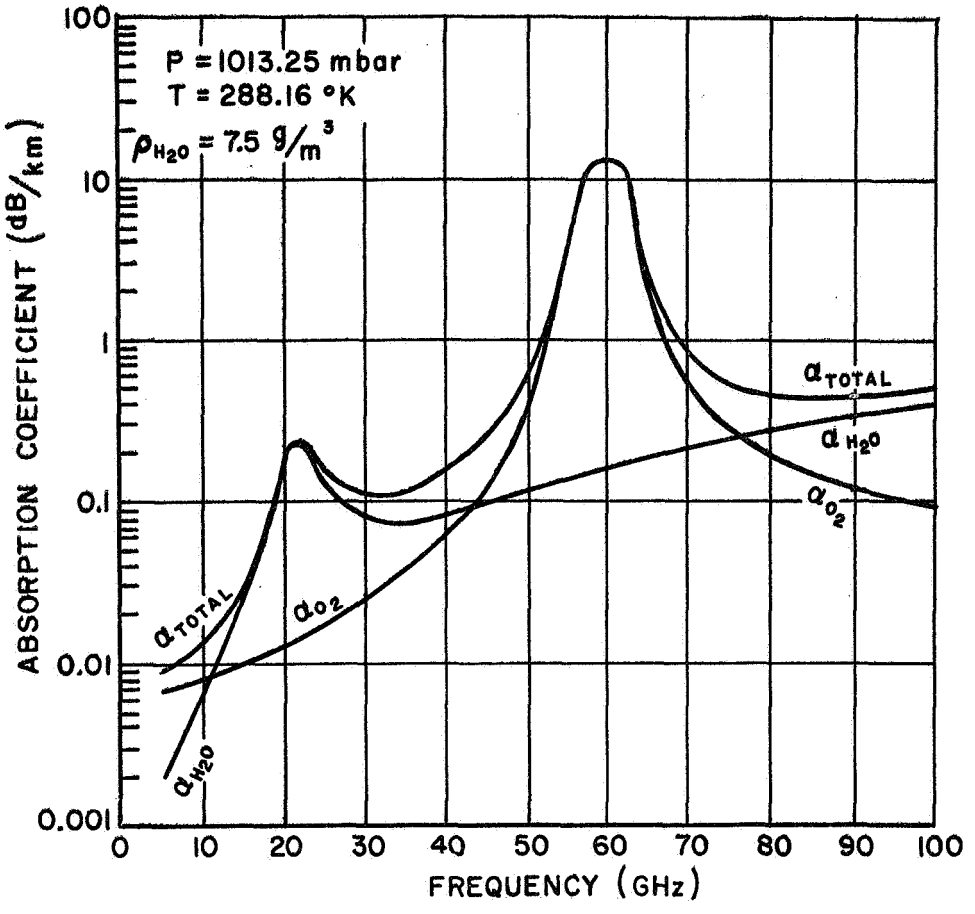

Fig. 7. Microwave absorption coefficients at standard surface conditions.

read from Fig. 8 and T_{eff} is the effective air temperature, given by $T_{eff} = 1.12\ T_{air} - 50^{0}K$ and T_{air} is the ground level thermometer temperature of the air. Thus $\tau_0 = -\log_e (1-T_{ant}/T_{eff})$ (see Fig. 9). For a horizontally stratified atmosphere it is a reasonably good approximation to assume that if τ_0 is the optical depth of the atmosphere at zenith, then at an angle of ϕ from the vertical the optical depth is $\tau_0 \sec \phi$ for $\phi < 85^{0}$. If a (h) and T(h) are known as a function of altitude h, Eq. (13) may be used to obtain T_{ant}. Further details are given in the references.

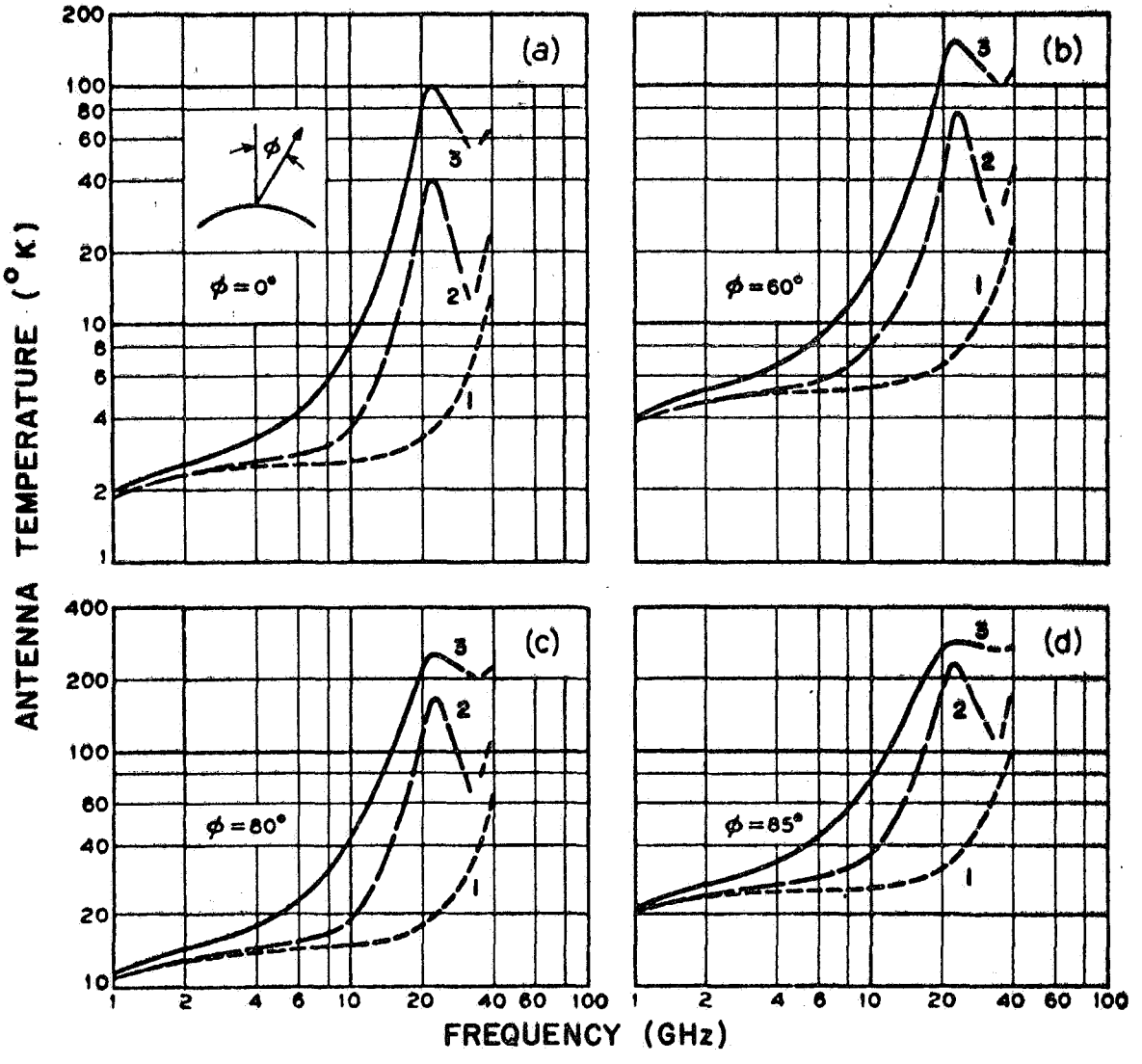

Fig. 8. Typical sky noise temperatures at various antenna positions for (1) very dry, (2) standard, and (3) humid summer atmospheres. (Copyright, The American Telephone and Telegraph Co., reprinted by permission.)

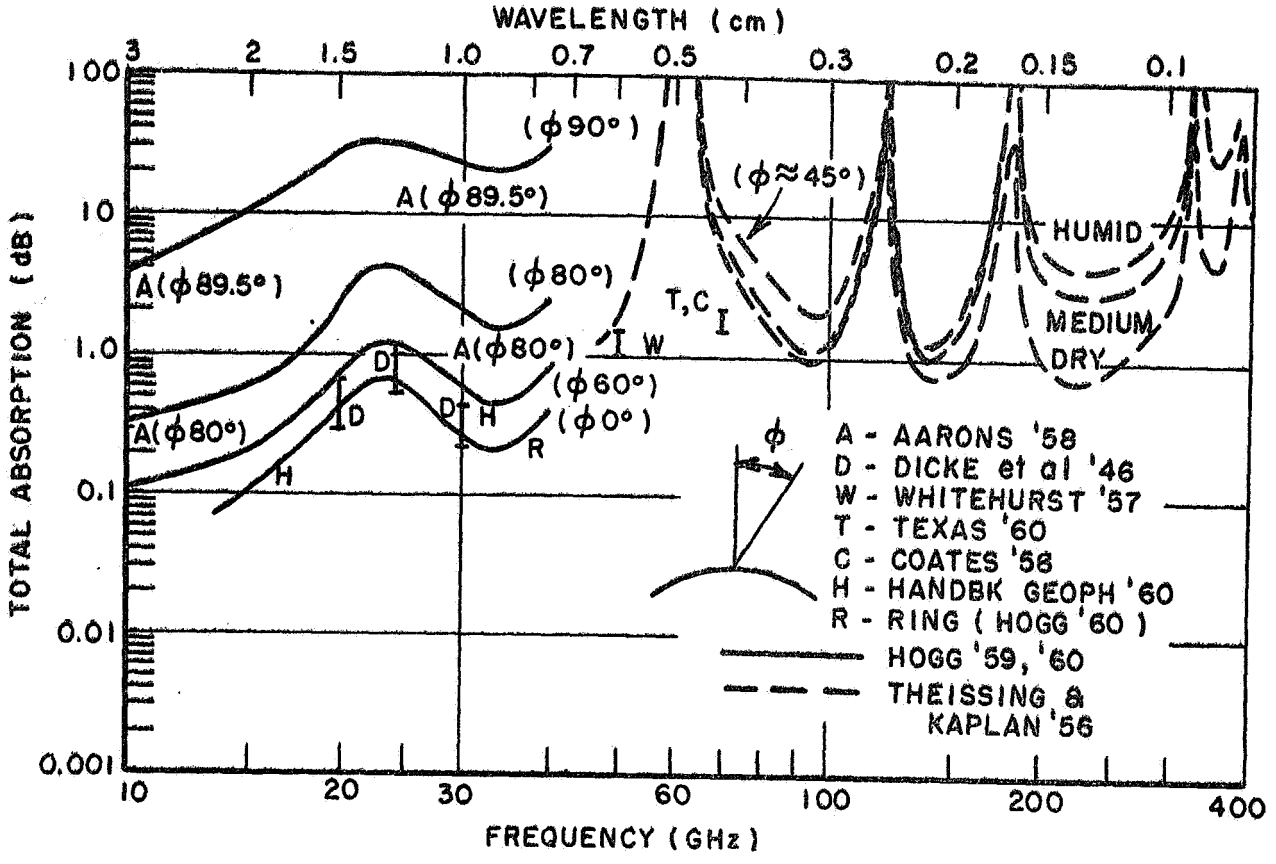

Fig. 9. Total absorption in decibels through the atmosphere (one way transmission) (after Meyer and Rosenbloom).

In addition to uncondensed water vapor, one must also consider (see Fig. 10) the effect of condensed water vapor, in the form of snow, rain, hail, clouds etc. Recent work is reviewed by Hunter, and by Hogg and Semplak. The attenuation data illustrates a further point. Throughout most of the microwave range (at least up to, say 16 GHz, and in the window at 35 GHz) not only the atmosphere, but even clouds and moderate rainfall are quite transparent so that imagery (albeit slightly degraded) can be obtained when visual or infrared observations are impossible.

Although the atmosphere is merely a nuisance to those interested in surface imagery, its properties are of great interest to meteorologists and oceanographers. Many important contributions to these sciences have already been made by microwave radiometry. It is the sensor of choice for many investigations, and it is significant that two of the three imaging radiometers now flying were developed for meteorologists and for the U.S. Coast Guard.

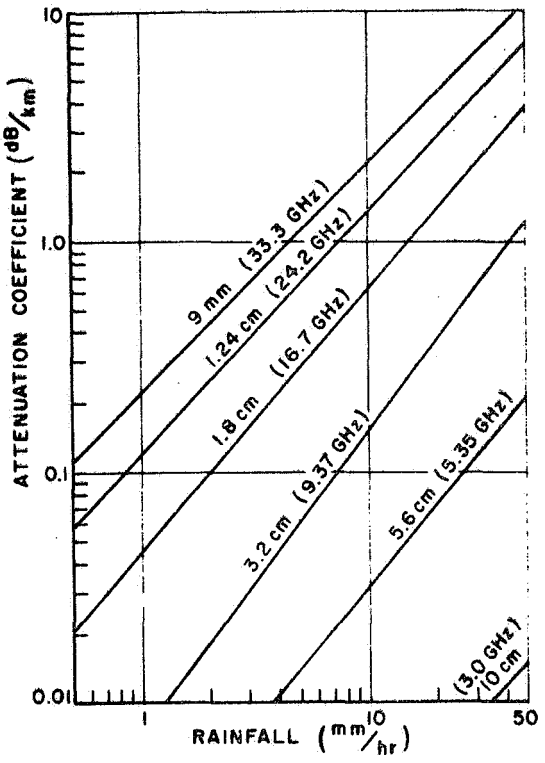

Fig. 10. Attenuation coefficient (dB/km) vs. rainfall rate for rain at 20°C. (Copyright, The Marconi Company Limited, reprinted by permission.)

V. APPARENT TEMPERATURES OF THE EARTH'S SURFACE. EMISSION, REFLECTION: ROUGHNESS AND DIELECTRIC CONSTANT EFFECTS

With the background of the preceding sections it is now possible to discuss the brightness temperature of the surface of the earth, since this is the parameter it is desired to image. Although ultimately determined by the surface roughness, the complex dielectric constant and the physical temperature of the surface (the latter two varying with depth) it is simpler to consider first two derived surface parameters, the emissivity and the reflectivity. These in turn are best defined in

terms of the differential scattering cross section of the surface (see Fig. 11).

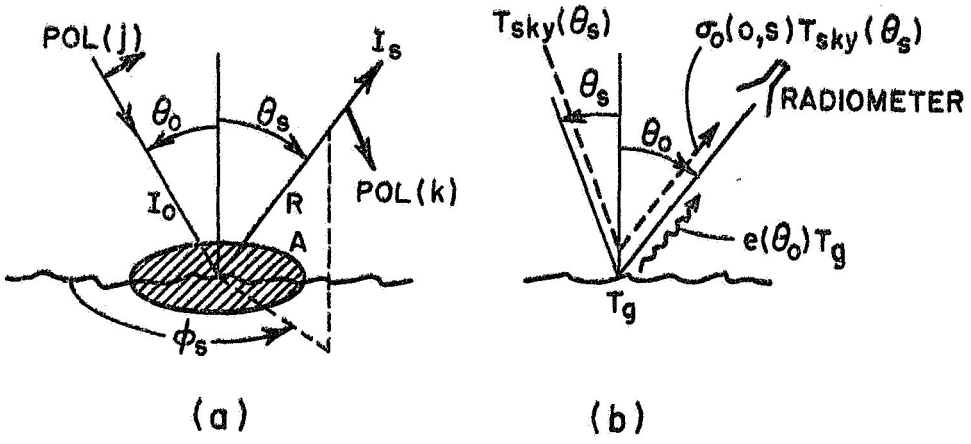

Fig. 11. Geometry for scattering and radiometer measurements.

Consider a small section of terrain of area (A), illuminated by a plane wave of intensity I_o watts/metre^2 and of some particular polarization state j. If we consider the energy scattered by the surface in a given direction $\theta_s\phi_s$, the intensity I_s of the component scattered with polarization state k at distance R will be given by

$$4\pi R^2 I_s \equiv \sigma_{jk}(o,s)\, I_o A \tag{20}$$

The proportionality constant $\sigma_{jk}(o,s)$ is called the differential scattering cross section per unit area of terrain. The subscripts jk indicate the state of the incident (j) polarization, and which state (k) of the scattered polarization is under consideration. The parameters (o,s) indicate direction from which (o means θ_o) the incident wave comes and into which (s means θ_s,ϕ_s) the scattered radiation goes. It is a consequence of the Lorentz reciprocity condition that

$$\sigma_{jk}(o,s) = \sigma_{kj}(s,o) \tag{21}$$

It is easy to see that the total scattered power is

$$(22) \qquad P_s = \int_0^{\pi/2} d\theta_s \int_0^{2\pi} d\phi_s \, [I_s R^2] = \int I_s R^2 d\Omega_s$$

Since the power falling on area A is $I_0 A \cos \theta_0$, we can define an albedo

$$(23) \qquad A_j(\theta_0) \equiv \frac{\text{Total scattered power}}{\text{Total incident power}} = \frac{1}{4\pi} \frac{\int(\sigma_{jk} + \sigma_{jj}) I_0 A \, d\Omega_s}{I_0 A \cos \theta_0}$$

for radiation incident from θ_0, polarization j. (The total scattered power includes both polarizations). Since what is not scattered is absorbed, the absorption coefficient becomes

$$(24) \qquad a_j(\theta_0) = \frac{\text{Total power absorbed}}{\text{Total power incident}} = 1 - A_j(\theta_0)$$

$$= 1 - \frac{1}{4\pi} \sec \theta_0 \int (\sigma_{jk} + \sigma_{jj}) d\Omega_s$$

Thus the absorption coefficient is 1 minus a weighted average of the bistatic scattering coefficients σ. We are next concerned with how much power is emitted by the surface by virtue of its temperature, T_g. Suppose the surface were an ideal black body; it would emit a certain power per unit solid angle per unit area per unit frequency interval into the direction θ_0, with a certain polarization state j. Now the actual ground will emit less than a black-body, and can be described by an emission coefficient

$$(25) \qquad e_j(\theta) = \frac{\text{Power radiated by ground surface towards } \theta_0 \text{ with polarization j}}{\text{Power radiated by black body towards } \theta_0 \text{ with polarization j}}$$

From the principal of detailed balance, it can be shown that

$$(26) \qquad a_j(\theta_0) = e_j(\theta_0)$$

i.e., the emission coefficient is equal to the absorption coefficient. This is the correct form of Kirchhoff's law for the general surface. It implies that the emission coefficient can be found from the differential scattering cross section.

With these definitions, we can find the total brightness temperature of the ground, taking into account both its own emission and the sky radiation which falls on the ground and is reflected into the radiometer (see Fig. 11b). Consider an ideal high gain antenna looking at an area with a physical temperature T_g. If this were a black body, the radiometer would see a radiation temperature T_g. The real ground emits only $e_j(\theta_o)T_g$ (since temperature and power are taken to be proportional), and this is the ground contribution to the brightness temperature (of polarization j in direction θ_o). The sky contribution, representing the effects of clouds, rain, etc., as well as the atmosphere, is represented by the downward radiation temperature $T_{sky}(\theta_s)$ reflected (via the differential cross-section $\sigma_{jk}(s,o)$) into the receiver direction θ_o, and integrated over all sky directions. It can be shown that this component contributes a brightness temperature

$$\frac{\sec \theta_o}{4\pi} \int [\sigma_{jk}(,s) + \sigma_{jj}(o,s)] T_{sky}(s)\, d\Omega_s$$

Thus the brightness temperature at ground level seen by the radiometer is

$$(27)\quad T_j^b(\theta_o) = e_j(\theta_o)\, T_g + \frac{\sec \theta_o}{4\pi} \int [\sigma_{jk}(o,s) + \sigma_{jj}(o,s)] T_{sky}(s)\, d\Omega_s$$

where

$$e_j(\theta) = 1 - \frac{\sec \theta_o}{4\pi} \int [\sigma_{jk}(o,s) + \sigma_{jj}(o,s)]\, d\Omega_s$$

This is the basic expression upon which the interpretation of surface brightness temperature depends. In many circumstances involving clear air, or uniform moderate cloud cover, $T_{sky}(\theta_o)$ can be written as

$$(28)\quad T_{sky}(\theta_o) = (1.12\, T_{air} - 50)\,(1 - e^{-\tau_o \sec \theta_o})$$

where τ_o, the zenith attenuation, can be estimated from Fig. 8 or Fig. 9. T_{air} and T_g are physical (thermometer) temperatures. Equation (27) is sometimes written in the form

$$(29)\quad T_j(\theta_o) = e_j(\theta_o)\, T_g + \bar{\rho}_j(\theta_o)\, \bar{T}_{sky}$$

It is clear from the correct expression (27) that here $\bar{\rho}_j$ and $\bar{T}_{sky}$ must represent some type of weighted average ground reflectivity and sky radiation temperature. Consistent definitions of $\bar{\rho}$ and $\bar{T}_{sky}$ are not available. In particular, it cannot be assumed that $\bar{\rho} + \bar{e} = 1$ except in certain special cases (flat surface, flat layers, etc.).

From this brief discussion one sees that the key to understanding the variations in radiation temperature of terrestrial surfaces lies in the differential cross-section σ_{jk}. The next few paragraphs consider the effects of roughness and dielectric constant on this parameter.

Smooth Ground

The simplest type of ground is one that is perfectly flat. In this case the ground acts like a specular reflector, i.e., the σ_{jk} are zero unless $\phi_s = \pi$ and $\theta_o = \theta_s$. In this case the radiation temperature of the ground is given by

$$(30) \qquad T_j^b(\theta) = (1 - |R_j|^2)T_g + |R_j|^2 (1 - e^{-\tau_o \sec \theta_o})T_{eff}$$

where R_j are the Fresnel coefficients for horizontal (perpendicular) and vertical (parallel) polarization,

$$R_h = \frac{\cos\theta_o - \sqrt{\varepsilon_r - \sin^2\theta_o}}{\cos\theta_o + \sqrt{\varepsilon_r - \sin^2\theta_o}} \quad ; \quad R_v = \frac{\varepsilon_r \cos\theta_o - \sqrt{\varepsilon_r - \sin^2\theta_o}}{\varepsilon_r \cos\theta_o - \sqrt{\varepsilon_r - \sin^2\theta_o}}$$

and ε_r is the complex relative dielectric constant. For circular polarization, or other linear polarizations, the appropriate reflection coefficients may easily be found in terms of R_h and R_v; however, it must be remembered that the polarization state of the incident wave is not preserved in these other cases, i.e., there would be a cross-polarized contribution to the sky reflection terms. An excellent example of the behavior of a smooth surface is shown in Fig. 12. Here the three sets of data represent measured brightness temperatures for asphalt, glacially polished limestone (Marblehead, Ohio) and a smooth coal bed exposed by strip mining operations (Cadiz, Ohio). The three curves represent the brightness temperatures computed from Eq. (30), using values of dielectric constant appropriate to the actual surfaces. It is clear that not only is there good agreement between measured and computed temperatures, but that such measurements offer a means for remotely sensing the value of the dielectric constant when exposed surfaces are available.

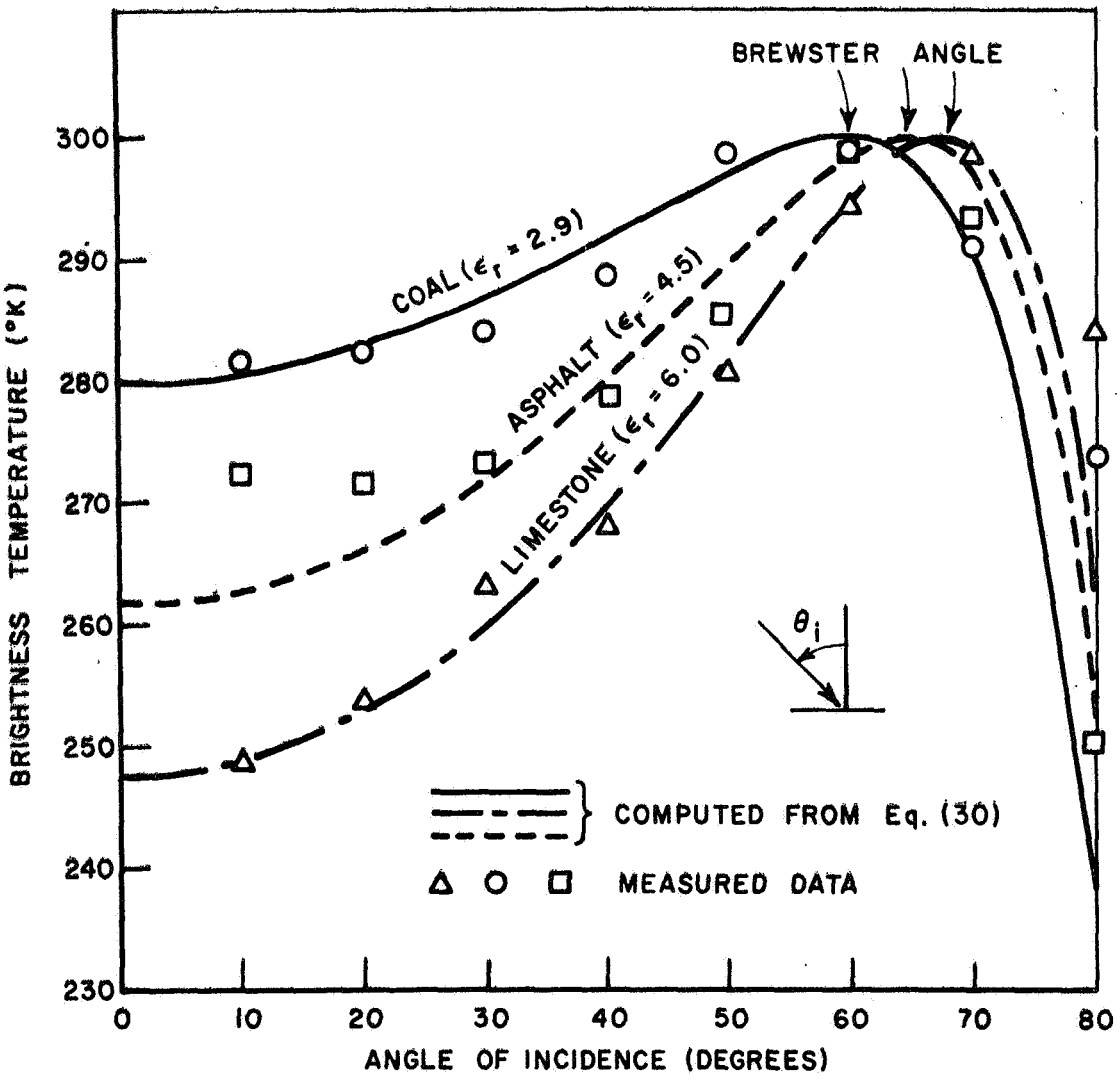

Fig. 12. Computed and measured brightness temperature of coal (near Cadiz, Ohio), limestone (near Marblehead, Ohio), and asphalt surfaces at 10 GHz, vertical polarization. (Data normalized to 300°K at the Brewster angle).

A number of slightly more complex surfaces, for example surfaces composed of uniform layers of different ε_r can also be handled by (30), where R is to be replaced by the reflection coefficient appropriate for the multilayer structure. An interesting example of a layered surface is shown in Fig. 13, where the oscillation in radiation temperature due to changes in the reflection coefficient with layer thickness are clearly apparent.

A second class of surfaces which can be handled by formulas like (30) are those, such as the surface of the sea, or sand dunes, where the gross surface is continuous with relatively gentle slopes, and there is little or no roughness of scale size the order of wavelength. In this case the surface acts locally like a specular reflector with tilted normal. The bistatic cross section shows a sharp lobe, or beam, in the specular direction for the average surface, with the beamwidth approximately equal to the rms surface slope. The Fresnel coefficients must be averaged over the slope distributions, a rather tedious process. The result in a typical case, see Figs. 14a, 14b, is to reduce the contrast between vertical and horizontal polarization. Here it is less clear that unambiguous information about either temperature or dielectric constant can be obtained unless something is known of the slope distribution.

A Digression in Dielectric Constants

Because of the key role played by the complex dielectric constant in determing the apparent temperature of smooth surfaces; because it controls the depth from which emission takes place; and because it is often related to properties such as density or water content, a brief survey is appropriate. The electrical properties of matter at microwave frequencies are described by the complex number $\varepsilon_r = \varepsilon' - j\varepsilon''$ (where ε' and ε'' are the real and imaginary parts, respectively). Often the complex dielectric constant is written in the form

$$\varepsilon_r = \varepsilon' - j\varepsilon'' - j\frac{\sigma}{\omega\varepsilon_0}$$

where σ is the d.c. conductivity (mhos/meter), ε_0 is the permittivity of free space, and $\omega = 2\pi f$. In this case the term ε' is proportional to the displacement current, the term ε'' accounts for dielectric losses, and the term $\sigma/\omega\varepsilon_0$ describes the effect of the dc conductivity (conduction current) in an alternating field. In fact, except at D.C., only the combination $(\varepsilon'' + \sigma/\omega\varepsilon_0)$ can be measured, so the division of the loss term into two parts is somewhat arbitrary. In the following, the conduction current term will be lumped in with ε'' unless explicily indicated, since at microwave frequencies it is usually dominated by dielectric losses. An alternative notation for the loss term is via the loss tangent, tan δ, with $\varepsilon_r = \varepsilon' (1 - j \tan \delta)$, i.e., $\varepsilon'' = \varepsilon' \tan \delta$.

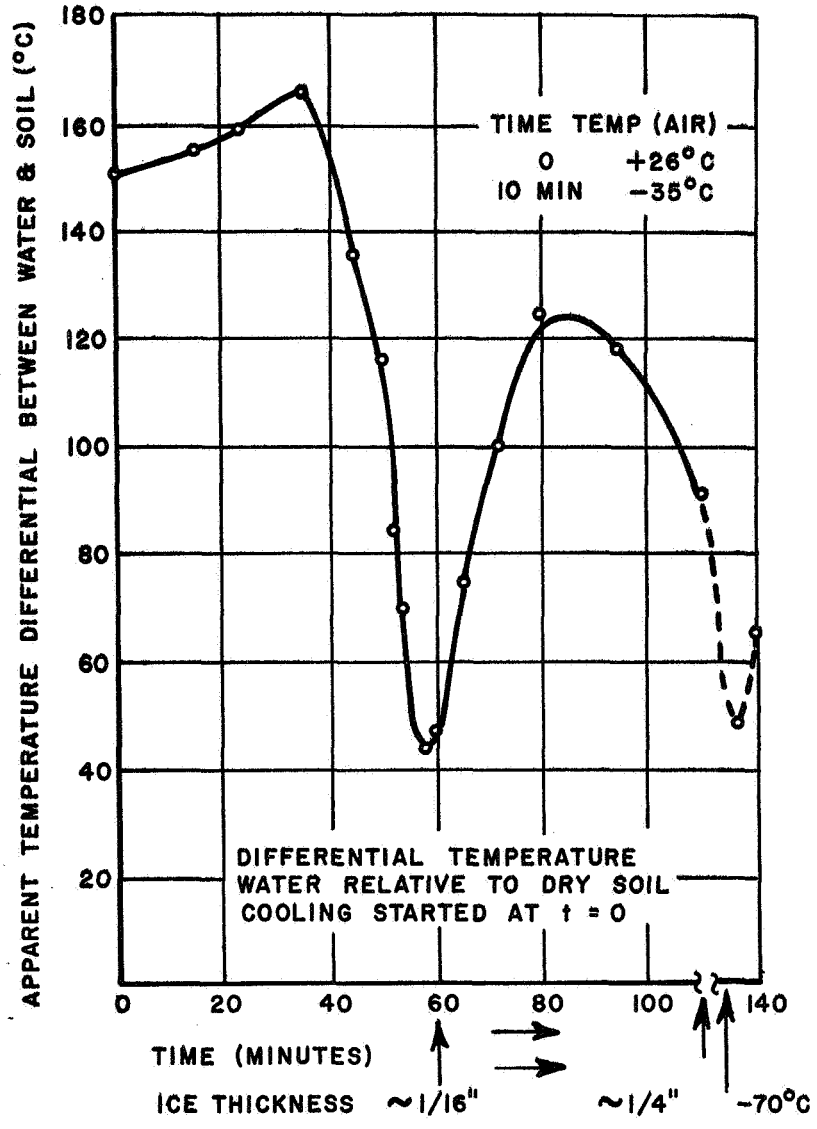

Fig. 13. Brightness temperature variation of a water surface covered by a layer of ice. (Pascalar and Sakamoto.) Third Symposium on Remote Sensing, University of Michigan, 1964.)

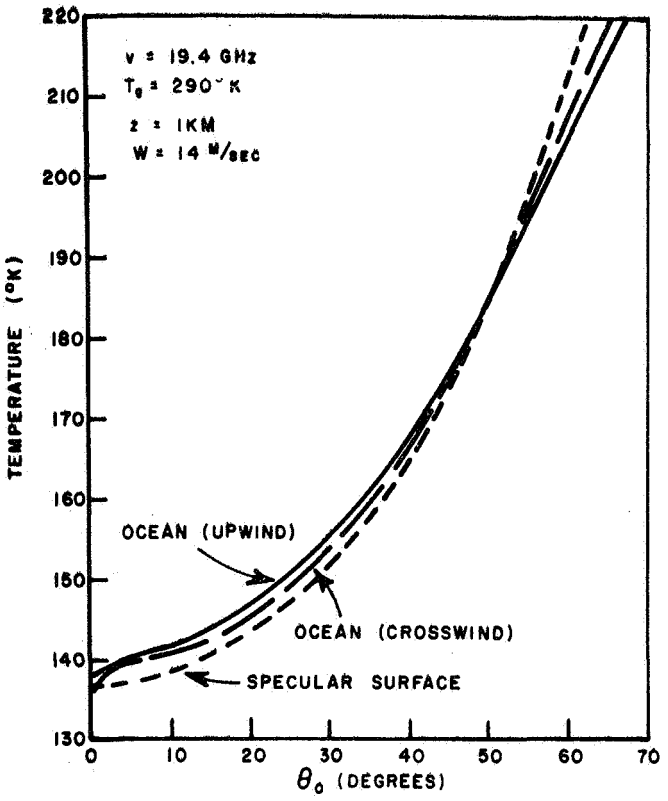

Fig. 14a. Vertically polarized component of the brightness temperature of the sea surface vs. incidence angle for a wind velocity of 14 m/sec. (After Stogryn.)

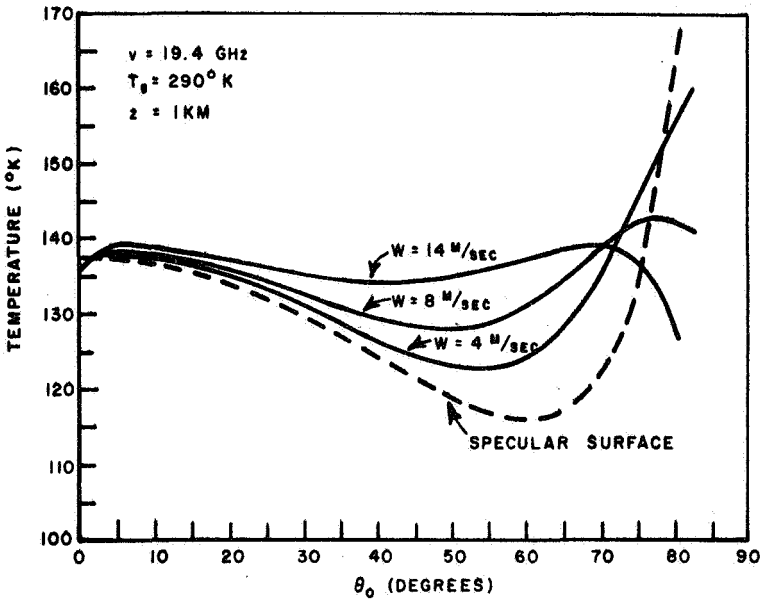

Fig. 14b. Horizontally polarized component of the brightness temperature of the sea surface vs. incidence angle for several wind velocities. (After Stogryn.)

If we consider a plane wave propagating in the z direction in a medium with dielectric constant ε_r it will have the form $e^{-\gamma z + j\omega t}$ where the complex propagation constant γ is written

$$\gamma = \alpha + j\beta = \omega\sqrt{\mu\varepsilon} = \frac{2\pi}{\lambda_0}\sqrt{\mu_r\varepsilon_r} = \frac{2\pi}{\lambda_0}\, n^*$$

where

λ_0 is the wavelength in vacuum

μ_r is the relative magnetic permeability (assumed to be 1)

n^* is the complex index of refraction

β is the propagation constant or wave number in the medium

α is the attenuation constant.

The wavelength in the medium is $2\pi/\beta$; the skin depth of the medium is $\delta = 1/\alpha$. (Note the parameter a(z) used in the discussion of atmospheric absorption is 2α, since it represents power loss). The skin depth δ is a useful parameter since it indicates how far a wave penetrates into a medium before its intensity is reduced to $1/e^2$, and thus what the thickness of the layer is from which the thermal radiation emanates.

Unfortunately, the measurement of ε_r at microwave frequencies, particularly for substances with small loss tangents, is quite difficult. A number of measurements are collected in Table I. It will be seen that ε_r does not vary greatly, though it has a tendency to increase with density; (for certain silicate rocks, e.g., pumice, the relation $\sqrt{\varepsilon_r} - 1 \simeq \rho/2$, where ρ is the density, holds quite well). The loss tangent, on the other hand, can vary over several orders of magnitude. Penetration may vary from several meters for dry sand, to a few millimeters for wet soil in the millimeter wavelength range (see Fig. 15).

In fact water plays a role of great importance in determining the dielectric behavior of soils, and other porous materials, and also of vegetation. The dielectric constant of distilled water and also of sea water, (where the conduction term enters) is shown in Fig. 16. Ice (see also Fig. 17) follows almost the same curve except that the frequencies involved are in KHz rather than GHz. Because water has a simple polar molecule, the dielectric constant has the form

$$\varepsilon_r = \varepsilon_\infty + \frac{\varepsilon_d - \varepsilon_\infty}{(1 + jf/f_0)} - j\,\frac{\sigma}{\omega\varepsilon_0}$$

where

σ = 4 ($\pm$2) mhos/meter for sea water; negligible for distilled water

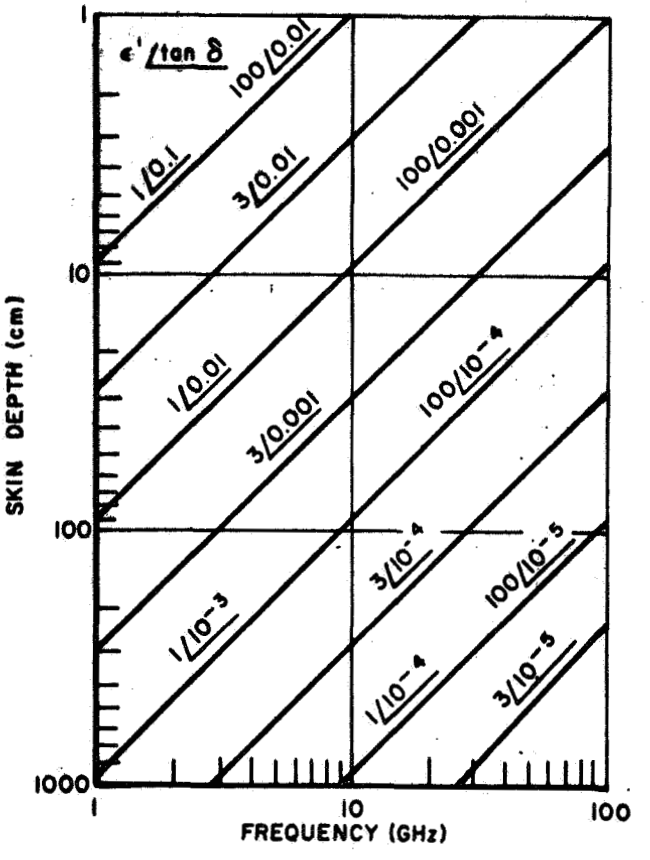

Fig. 15a. Skindepth vs. frequency for various values of $\varepsilon'\tan\delta$.

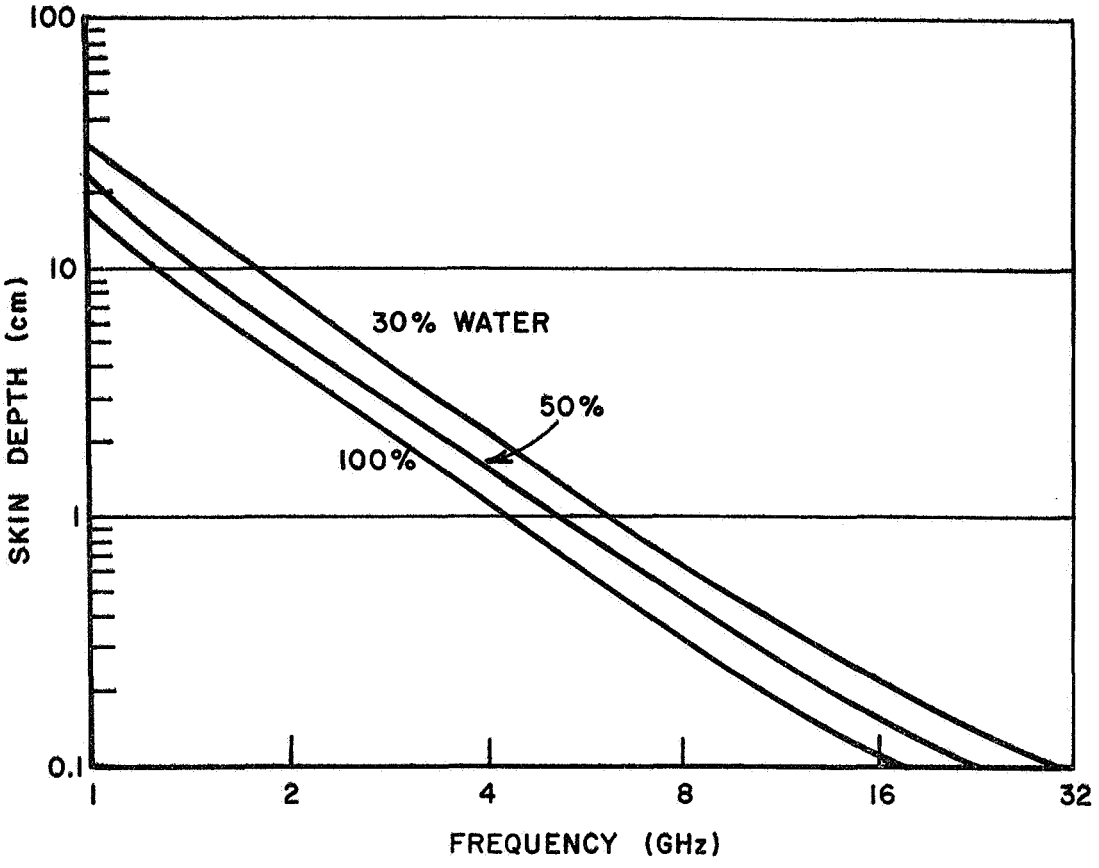

Fig. 15b. Skindepth vs. frequency for water (100% curve) and for media whose dielectric constant is 50% and 30% respectively of the dielectric constant of water.

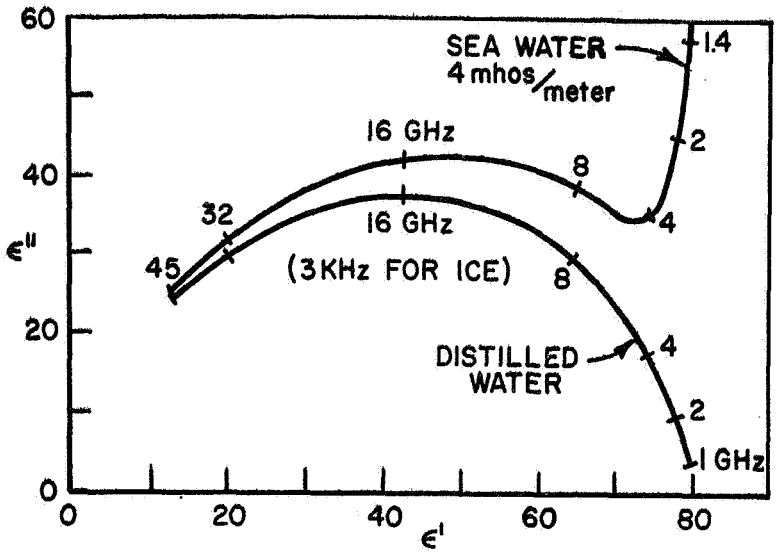

Fig. 16. Relative complex dielectric constant of water.

ε_∞ = 5.5 for water and 3.2 for ice
ε_d = 87.7 - 0.4 (T-273) for water ($T_{in}{}^{o}K$)
ε_d = 90 + T /550 for ice ($T_{in}{}^{o}C$)
f_o = 3 KHz for ice at 263°K
f_o = 9.1 GHz for water at 273°K
f_o = 12.6 GHz for water at 283°K
f_o = 17.2 GHz for water 293°K
f_o = 21.6 GHz for water 303°K

The fact that the relaxation frequency f_o is temperature dependent means that emissivity is a function of temperature as well as look angle. Figures 18 and 19 show the dielectric constant for several soils as a function of moisture content. It is clear that the moisture content has a decisive influence on both ε_r and the emissivity. This is the basis for the expectation that microwave imagery may provide a means for monitoring soil moisture. An idea of the penetration depth in water and in wet soils may be found from Fig. 15b.

The dielectric constant of vegetation also depends on the water content, as can be seen from Fig. 20. Here again there is the expectation that crop moisture can be monitored by the sensor.

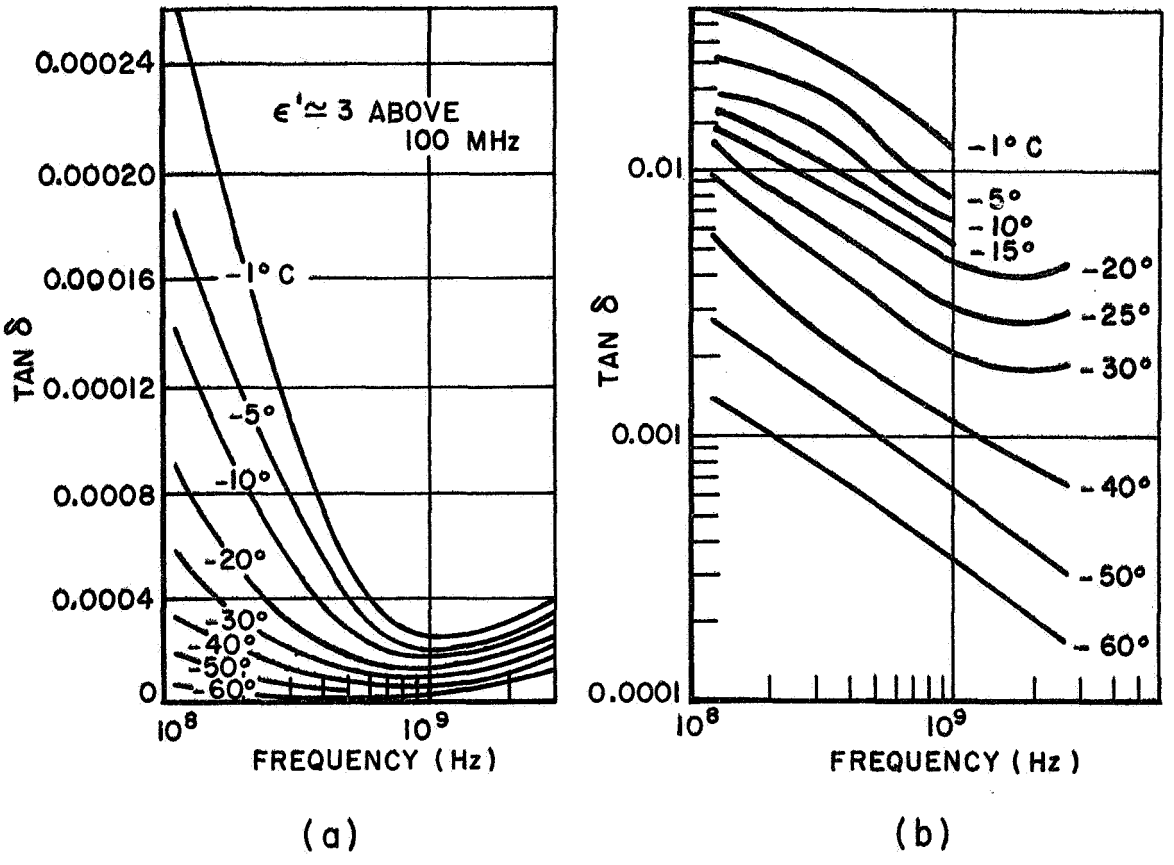

Fig. 17. Loss tangent of ice vs. frequency with temperature as parameter. ((a) Firm ice, (b) Sea ice.) (After Iglesias and Westphal.)

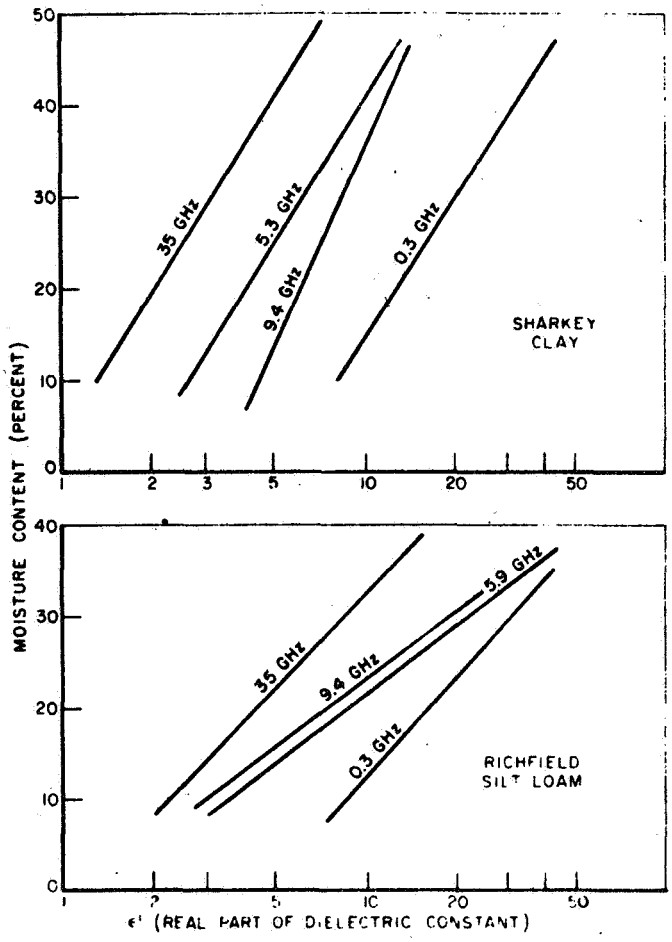

Fig. 18. Relative dielectric constant of soils vs. moisture content. (After Lundien.)

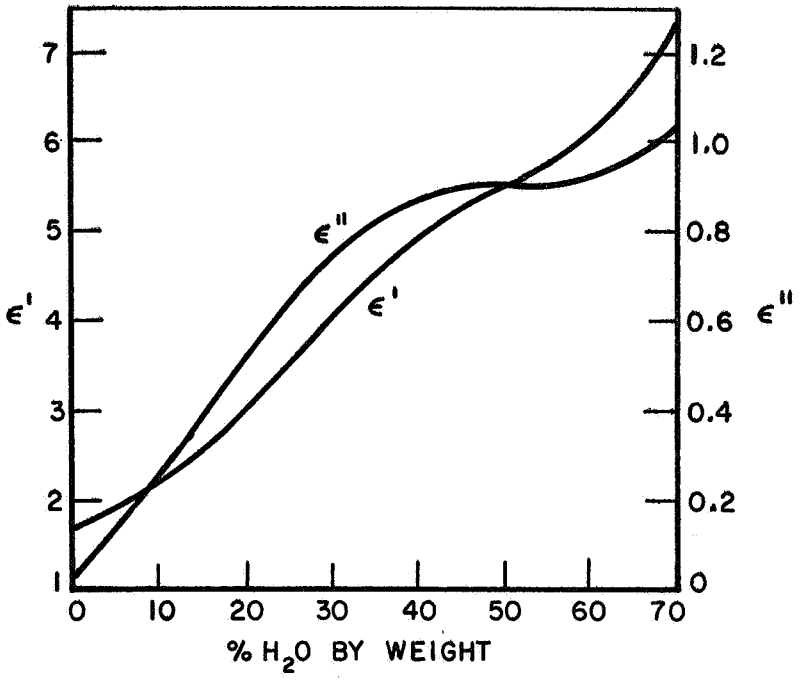

Fig. 19. Dielectric constant for Fuller's earth vs. per cent water by weight at 8.5 GHz. (After Iglesias and Westphal.)

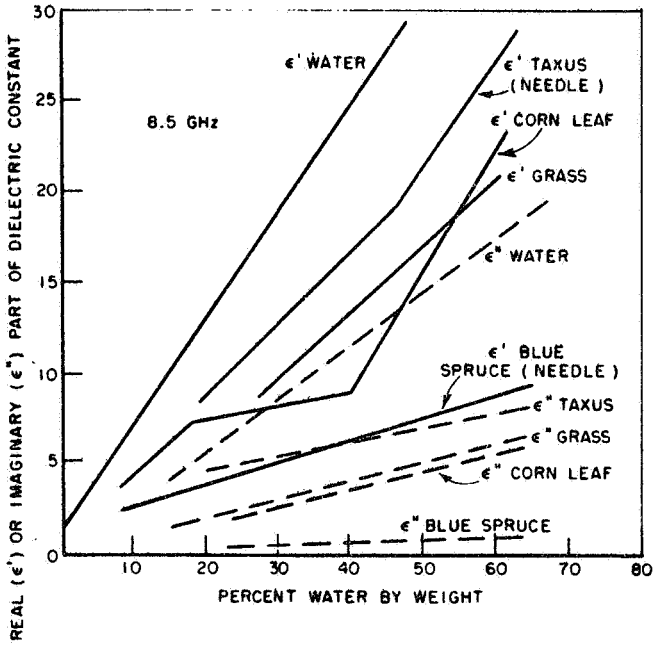

Fig. 20. Relative dielectric constant of vegetation at 8.5 GHz. (Carlson)

Diffuse Surfaces

The second major class of surfaces for which the emissivity, reflectivity and radiation temperature can be estimated is the diffusely scattering surface (e.g., vegetation or crushed rock) for which $\sigma_{jk}(o,s)$ is more or less isotropic. The calculation of σ_{jk} is extremely difficult, so it is convenient to use simple empirical laws to describe the scattering function. A number of these are collected in Table II. Although somewhat similar in appearance, there are slight theoretical reasons for preferring one or the other for particular surfaces. The Lambert law seems particularly appropriate for surfaces of large blocks or chunks of material (e.g., parts of the lunar surface, Mono craters) with many reentrant surfaces and cavities. The Lommel-Seeliger Law was derived for a "surface" of many layers of independent scatterers, and is more appropriate for vegetation. All these models are characterized by a single numerical parameter (Γ), which in practice may depend on the frequency. (For example, for vegetation, it depends on the ratio of leaf-size to wavelength and thus decreases with frequency; and on the dielectric constant, so increases with moisture content.)

For a standard atmosphere the Lambert and "Grass" laws can be integrated in closed form. However, a better comparison of the models may be obtained from Fig. 21, which shows the reflected sky contribution for each model and also the emissivity contribution, (the latter shown as the difference between surface temperature T_g and the brightness temperature).

A number of diffuse surfaces can be accomodated quite well by these models. In analysing the apparent temperature measurements it is helpful to recall that the predicted temperatures will depend on the parameter Γ in Table II. This parameter in turn can be found from the back-scattering cross section (i.e., the radar return) of the surface if this is known. For example, Fig. 22b indicates the back-scattering parameter $\gamma(\theta_o) = \sec\theta_o\ \sigma_o(\theta_o)$ for large blocks of pumice. It is seen that the scattering is almost independent of frequency (as contrasted, for example, to the back-scattering from the relatively smooth lapilli surface in Fig. 22a) and follows fairly well the angular dependence expected of a Lambert surface. The parameter Γ is approximately 0.1. The apparent or brightness temperature of this same surface is shown in Fig. 23 for both 10 GHz and 35 GHz (the curves labelled "light"). The measured brightness temperature is almost independent of angle, as required for a Lambert surface, and implies an emissivity in fairly good agreement with the value $e = 1 - \Gamma/4 = 0.975$ expected from the back-scattering measurements. A similar analysis could be made for the pair of graphs shown in Figs. 24 and 25, using the Lommel-Seelinger or the "Grass" scattering laws. Again, there is qualitative agreement between measured apparent temperature and that calculated from the backscattering parameter Γ inferred from the radar return measurements.

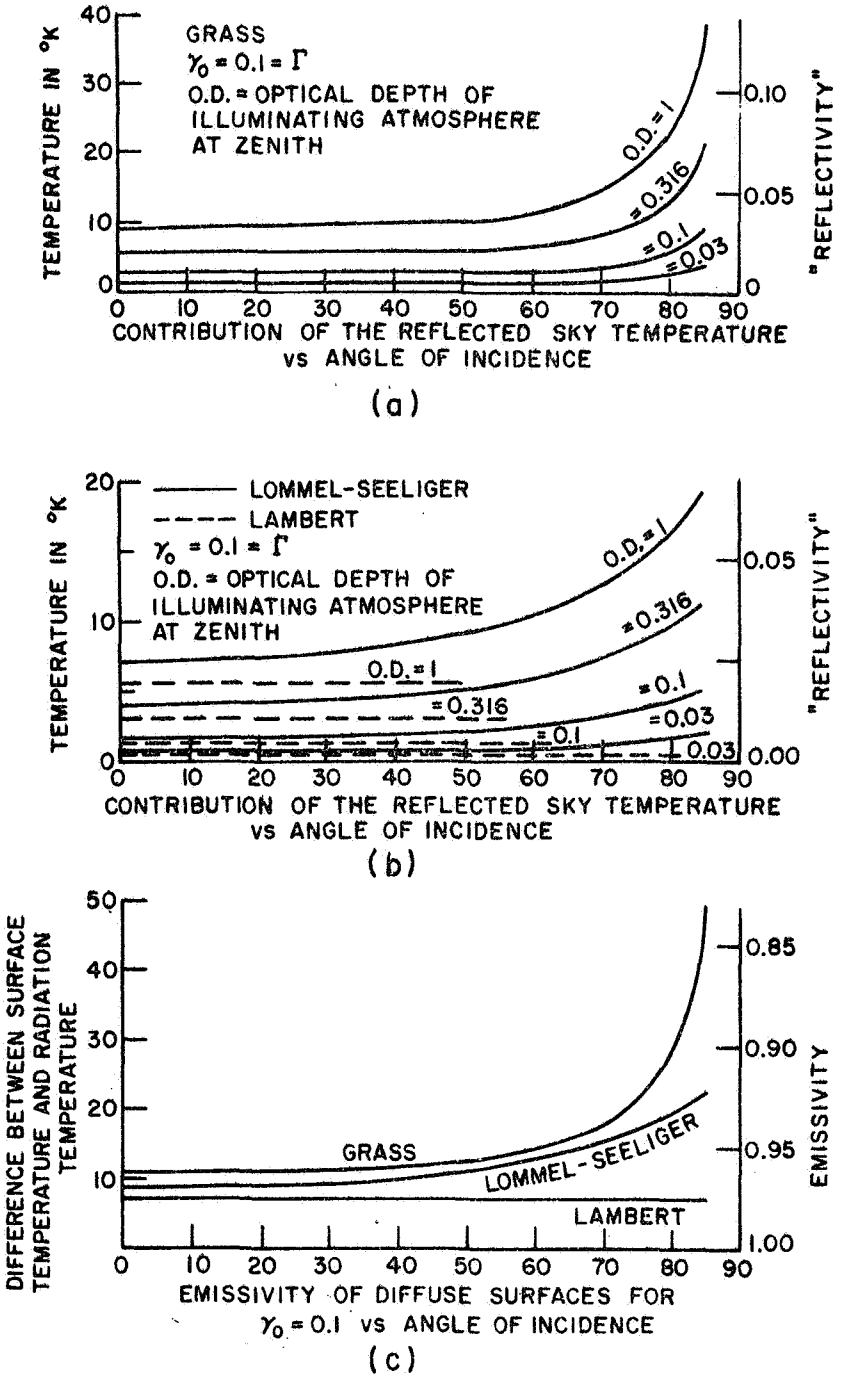

Fig. 21. Emissivity and reflected sky temperature contributions to the brightness temperature of a diffuse surface for three empirical scattering laws.

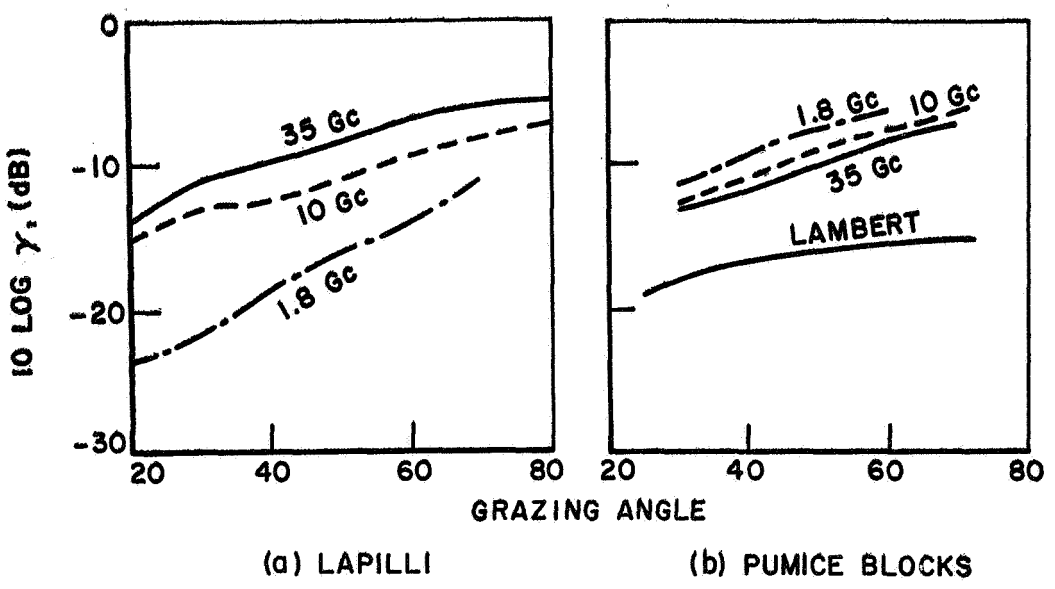

Fig. 22. Back scattering from smooth and rough pumice surfaces.

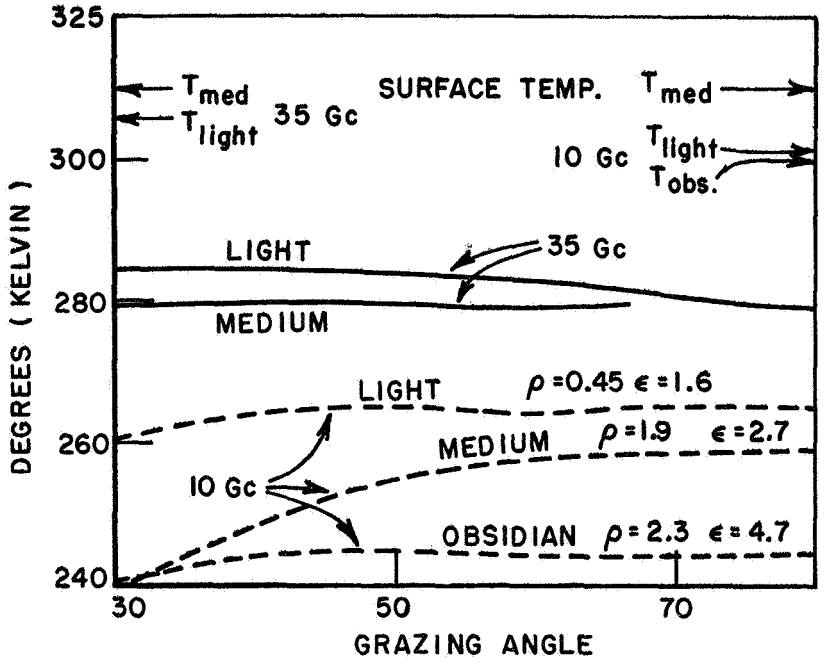

Fig. 23. Brightness temperatures of pumice blocks of various density and dielectric constant.

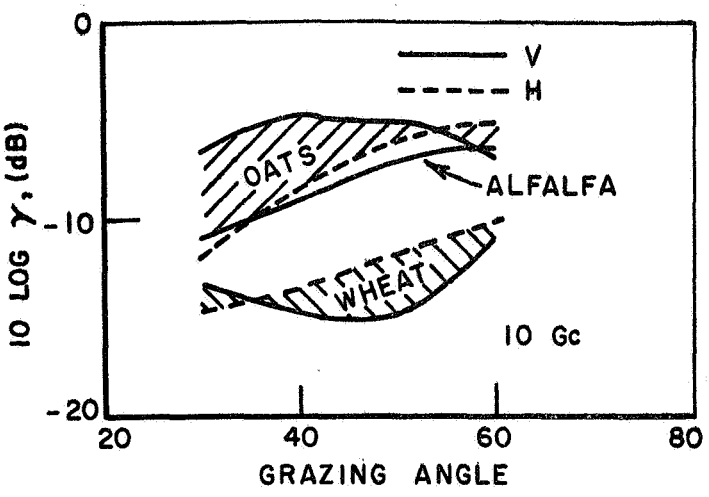

Fig. 24. Back scattering from vegetation surfaces of 10 GHz.

Many surfaces of interest, unfortunately, do not fall into the simple categories of "specular" or "diffusely rough", either because they are composite (e.g., a sparsely vegetated sand dune) or because they contain multiple roughness scales. Such surfaces must be handled empirically at the present time.

VI. APPLICATIONS OF MICROWAVE RADIOMETRY

The principal scientific applications of microwave radiometry have been made, up to the present, in the field of meteorology. Because the absorption and emission of molecular oxygen and water vapor, and the scattering properties of the major atmospheric particles (rain, snow, clouds, hail) change rapidly with frequency in the microwave region, the judicious choice of frequency can emphasize the contribution of one component or another. Current research centers around the frequencies near 22 GHz for studies of the water vapor distribution, 60 GHz for the temperature profile of molecular oxygen, and 19 GHz for imager studies of condensed water in the atmosphere.

The principal technical application has been the program of iceberg surveys initiated by the U.S. Coast Guard with a 13 GHz airborne imaging radiometer. Images have also been used in the study of sea ice distributions. Suggested applications have included synoptic measurements of the temperature of the surface of the ocean, passive aids to navigation

from aircraft or satellite altitudes, etc. A number of other possible applications are mentioned in the Symposia proceedings listed in the bibliography.

Most of the systematic studies of interest to geoscientists have been concerned with the role of water in modifying the apparent temperature of relatively smooth surfaces. For example, the development of a layer of ice over a freezing water surface can be effectively monitored (see Fig. 13) by the apparent temperature changes; and diurnal and other changes in the relative moisture content of snow can be similarly observed. The large influence of water content on the dielectric constant of soils noted in Figs. 18 and 19 makes it possible, under appropriate conditions, to determine the moisture content of the soil from brightness changes, as can be seen from the interesting curves in Fig. 26. In a rather similar way (see Fig. 20) changes in the moisture content of vegetation can change the dielectric constant considerably. In Fig. 25 it can be seen that wheat and oats (although very similar in structure), have significantly different emissivities, and it seems likely that this must be in part a consequence of the difference in moisture content of the two crops.

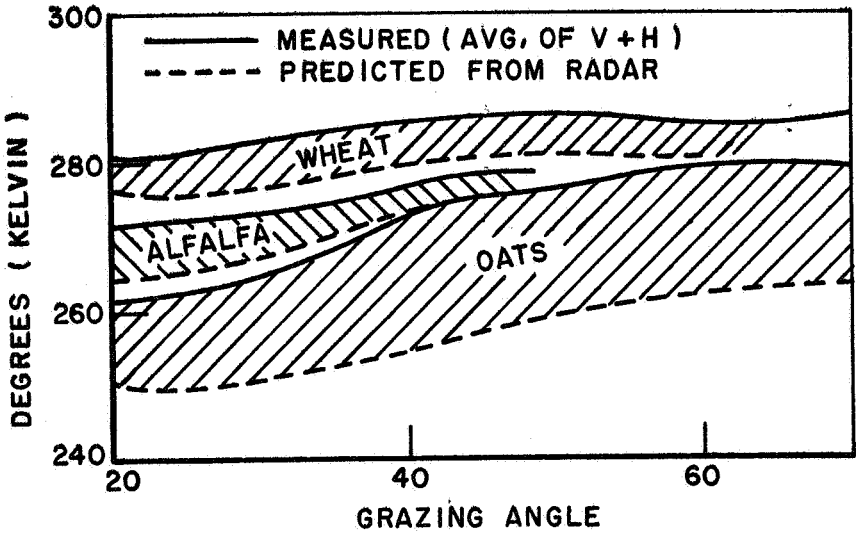

Fig. 25. Brightness temperatures of the surfaces of Fig. 24 compared with predicted brightness temperatures.

A second area of interest is the determination of the dielectric constant of exposed rocks. For example, if the exposed surface is smooth, one would expect (see Fig. 12) to be able to determine the dielectric constant either from the Brewster angle or from the brightness temperature at normal incidence.

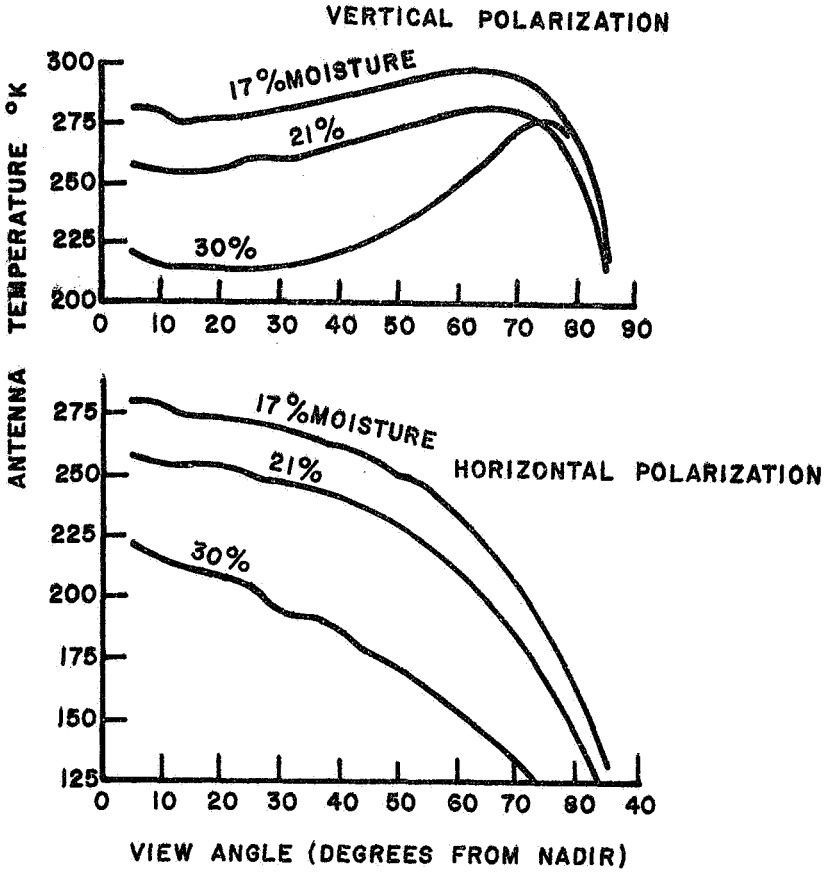

Fig. 26. Brightness temperature of soil vs moisture content (after Kennedy and Edgerton).

Even for diffuse surfaces it may be possible to estimate the dielectric constant if some a priori information is available. For example Fig. 23 shows the apparent temperature of three areas in the Mono craters, one covered by a very light pumice, one by a pumice of medium density and the third by obsidian. Since the denser obsidian has a higher dielectric constant it is a better reflector, and appears cooler than the lighter material. Evidently these particular pumices can be classified as to dielectric constant, and thus density, on the basis of their apparent temperatures.

VII. CONCLUSIONS

There is one significant feature that persists through all the applications described in the previous sections. They involve comparisons, either in time, or in look angle, or between one surface and a closely related one. Because of the many factors influencing the brightness temperature of a surface - the distribution of physical temperature with depth, the skin depth, the surface roughness, the dielectric constant, etc. - it is usually not possible to say much about a surface on the basis of a few measurements or a single image. It would appear that the quantitative application of microwave radiometry, for example in monitoring soil or vegetation moisture, or even in remotely estimating the surface temperature, will depend on the use of a sequence of images of the same area, so that the complicating effects of the surface structure or roughness or the emissivity can be calibrated out. It is also apparent that in many cases, the significance of the interpretation of the sensor output is often much increased if one can also make use of the data from a complementary active sensor (i.e., radar). Thus the development of combined active-passive sensor systems for this purpose would be highly desirable.

Finally, it should be clear that while several interesting possibilities have now been opened for the radiometer as a remote sensor, one may expect the number and scope of its applications to multiply rapidly as imagery becomes more widely disseminated. This means, in turn, that the detailed, controlled studies for each particular application must occupy an increasingly important role in the development of the sensor as a quantitative instrument.

TABLE I

Sample	Freq. in GHz	ε_r	tan δ	Density	
1	35	2.3	0.08		Red Granite
2	35	2.4	0.06		White Granite Crushed
3	35	1.7	0.012		White Pumice Crushed
4	35	1.6	0.02		Black Pumice Crushed
5	1.0	35	0.175	3.01	Chondritic Meteorite
6	14	4.6	0.006	1.81	Halite
7	14	3.8	0.012	1.56	Halite
8	14	3.3	0.009	1.42	Halite
9	10	4	0.1		Limonite (Coarse)
10	10	4	0.01		Limonite (Fine)
11	8.5	3.3	0.0055	1.11	Magnesite Hard Packed
12	8.5	2.45	0.002	1.22	Quartz Powder
13	0.1	10	0.02		Basalt (Hawaii) Oven Dry
14	0.1	10	0.08		Basalt (Hawaii) 0.36% Wate
15	0.1	7 to 9	0.1		Granite (Quincy)
16	0.1	8.4	0.006 to .018	2.65	Limestone (Lucerne Valley)
17	0.1	5.5	0.001		Rhyolite
18	10	4.8	0.005	2.45	Basalt (Vesicular)
19	10	4.4	0.013	2.63	Biotite Granite
20	10	5.1	0.081	2.35	Obsidian
21	10	4.8	0.009	2.74	Olivine Basalt
22	10	5.4	0.086	2.68	Serpentine
23	10	5.0	0.027	1.62	Volcanic Ash
24	10	4.7	0.017	2.27	Altered Tuff
25	10	5.5	0.016	2.03	Tuff
26	10	4.7	0.01	2.3	Horn blende
27	10	3.0	0.012	0.78	Mono Pumice
28	14	2.9	0.011	1.63	Desert Sand
29	14	8.2 to 8.6	0.004 to .02	2.65	Limestone (Lucerne Valley)
30	14	4.7 to 6	0.01 to 0.1	2.35	Asphalt
31	14	4.5 to 5.2	0.02 to .06	2.1	Concrete
32	3	81	00.38		Maine Potato 80% Water

Data from Iglesias and Westphal
and J.D. Shaw and C.A. Barlow - AFCRL Report 64-74
(Radar Analysis of the Moon II - Surface Properties)
and other sources.

TABLE II

The Scattering Cross Section $\sigma_o(o,s)$ for Various Empirical Laws

Name	Bistatic Law	Backscattering Cross-Section	Albedo = 1-Emissivity
Lambert	$\Gamma \cos\theta_o \cos\theta_s$	$\Gamma \cos^2\theta_o$	$\Gamma/4$
Generalized Lambert	$\Gamma(\cos\theta_o \cos\theta_s)^n$	$\Gamma \cos^{2n}\theta_o$	$\frac{\Gamma \cos^{n-1}\theta_o}{2(n+1)}$
= Lommel-Seeliger (many layers of isotropic scatterers)	$\Gamma \frac{2(\cos\theta_o \cos\theta_s)}{\cos\theta_o + \cos\theta_s}$	$\Gamma \cos\theta_o$	$\Gamma[1-\cos\theta_o \log_e(1+\sec\theta_o)]$
Lommel-Seeliger with multiple scatter	———	$\Gamma \cos\theta_o[1-\cos\theta_o \log_e (1+\sec\theta_o)]$	———
"Grass" (Empirical Law)	$\Gamma \frac{\cos\theta_o + \cos\theta_s}{2}$	$\Gamma \cos\theta_o$	$\frac{\Gamma}{4}\left(1+\frac{\sec\theta_o}{2}\right)$
Single layer of isotropic scatterers	$\Gamma_1 = NA_K$	Γ_1	$(\Gamma_1/2)\sec\theta_o$

Γ, Γ_1 arbitrary constants

Angles θ_o, θ_s with respect to surface normal (not grazing angles)

VIII. BIBLIOGRAPHY

A. Radiometer Techniques

Ewen, H.I., "State of the Art of Microwave and Millimeter Wave Radiometric Sensors," Int. Symp. on Electromagnetic Sensing of the Earth from Satellites, Miami Beach, Florida, November 22-24, 1965.

Dicke, R.H., "The Measurement of Thermal Radiation at Microwave Frequencies," R.S.I. 17, 288, 1946.

Strum, P.D., "Considerations in High Sensitivity Microwave Radiometry," Proc. IRE, 46, p. 43, 1958.

Blinn, J.C. and James P. Campbell, "Microwave Sensing for Air Navigation," IEEE Trans. AES-2, 585, September 1966.

McGillem, C.D. and T.V. Seling, "Influence of Systems Parameters on Airborne Microwave Radiometer Design," IEEE Trans. Mil. Electronics, p. 296, October 1963.

Bracewell, R.N., "Radio Astronomy Techniques," Hand. der Physik, Vol. LIV, Springer, Berlin, 1962.

Twomey, C.H., "The Application of Numerical Filtering to the Solution of Integral Equations Encountered in Indirect Sensing Measurements,"J. Frank, Inst. 279, 95, 1965.

B. The Atmosphere

Barrett, A.H., "Microwave Spectral Lines as Probes of Planetary Atmospheres," Mem. Royal Sci. Liege 5th Ser. 7, 197-219, 1962.

Becker, G.E. and S.H. Autler, "Water Vapor Absorption of Electromagnetic Radiation in the Centimeter Wavelength Region, Phys. Rev., Vol. 70, No. 5, 300-307, 1946.

Croom, D.L., "The Possible Detection of Atmospheric Water Vapor from a Satellite by Observation of the 13.5 mm and 1.66 mm H_2O Lines," J. Atm. Terr. Phys. 28, p. 323, 1966.

Falcone, V.J., Jr., "Calculations of Apparent Sky Temperature at Millimeter Wavelengths," Radio Sci., Vol. I, No. 10, 1205-1209, 1966.

Hogg, D.C. and R.A. Semplak, "Effect of Rain and Water Vapor on Sky Noise at Centimeter Wavelengths," BSTJ, XL, 1331, September 1961.

Hunter, I., "Attenuation of Microwaves in the Troposphere," The Marconi Review, 3rd Qt., 122-142, 1964.

Staelin, D.H., "Measurement and Interpretation of the Microwave Spectrum of the Terrestrial Atmosphere Near 1 cm Wavelength," J.G.R. 71, 2875, 1966.

Symposium on Planetary Atmospheres and Surfaces, Radio Science 69D, p. 1513-1690, 1965.

Van Vleck, J.N., "The Absorption of Microwaves by Uncondensed Water Vapor," Phys. Rev., Vol. 71, No. 7, 425-433, 1947.

Van Vleck, J.N., "The Absorption of Microwaves by Oxygen," Phys. Rev., Vol. 71, No. 7, 413-424, 1947.

Westwater, E.R., "Ground-Based Passive Probing Using the Microwave Spectrum of Oxygen," Radio Science, 69D, No. 9, 1202-1211, (1965).

Wulfsberg, K.N., "Atmospheric Attenuation at mm Wavelengths," Radio Sci. 2 (New Series) p. 319, 1967.

C. Dielectric Properties

Hasted, J.B., "The Dielectric Properties of Water, in Advances in Dielectrics, Vol. 3, Wiley, 1961.

Iglesias, J. and W.B. Westphal, "Supplementary Dielectric Constant and Loss Measurements," Tech. Report No. 203, Lab. for Insulation Research, Massachusetts Institute of Technology, January 1967.

Lundien, J.R., "Terrain Analysis by Electromagnetic Means," Rpt. 3, Laboratory Responses to Simulated Terrain, U.S. Army Engineers, Waterways Experimental Station, October 1965.

D. Surface Temperatures

Hagfors, T. and J. Moriello, "The Effect of Roughness on the Polarization of Thermal Emission from a Surface," Radio Science 69D, p. 1616, 1965.

Peake, W.H., and S.N.C. Chen, "Apparent Temperatures of Smooth and Rough Terrain," IRE Trans. PGAP-9, 567, 1961.

Peake, W.H., "Interaction of Electromagnetic Waves with Some Natural Surfaces," IRE Trans. PGAP-7, Spec. Suppl., p. S324, December 1959.

Croom, D.L., "Naturally Occurring Thermal Radiation in the Range 1-10 Gcs.," Proc. IEE, 111, pp. 967-978, 1964.

Stogryn, A., "The Apparent Temperature of the Sea at Microwave Frequencies," IEEE Trans. AP-15, p. 278, 1967.

Straiton, A.W., C.W. Tolbert and C.O. Britt, "Apparent Temperature Distribution of Some Terrestrial Materials and the Sun at 4.3 mm Wavelength,"J.A.P., 29, p. 776, 1958.

E. Applications

Catoe, C.W., P. Nordberg, P. Thaddeus, G. Ling, "Preliminary Results from Aircraft Flight Tests of an Electrically Scanning Microwave Radiometer," NASA Rept. X-622-67-352, GSFC, August 1967.

Kennedy, J.M. and A.T. Edgerton, "Microwave Radiometric Sensing of Soil Moisture Content," Int. Union, Geod. and Geophys., 14th Gen. Assembly, September 27 - October 7, 1967, Berne, Switzerland.

International Symposium on Electromagnetic Sensing of the Earth from Satellites, November 22-24, 1965, Florida.

"Oceanography from Space," Woods Hole Ocean. Inst. WHOI No. 65-10, 1965.

Proceedings of the 1st, 2nd, 3rd and 4th Symposia on Remote Sensing of Environment (University of Michigan).

A.E. Ladely, "Radiometry for Ice Detection," The Engineer's Digest (USCG) No. 154, pp. 34-38, January, February, March, 1967.

J.C. Blinn, III, P. Chapman, J. Quade, "Airborne Multifrequency Microwave Sensing of an Exposed Volcanic Province," Tech. Mem. 33-405, Jet Propulsion Laboratory, October 15, 1968.

ACKNOWLEDGMENT

Parts of this report were originally prepared for a short course in Geological Remote Sensing held at Stanford University in December 1967, and I would like to thank the organizer Professor R.J.P. Lyon, for the opportunity to participate.